Lockheed

Missiles & Space Company, Inc.

HUNTSVILLE RESEARCH & ENGINEERING CENTER

Cummings Research Park
4800 Bradford Drive,
Huntsville, Alabama

PARAMETRIC ANALYSIS OF DIFFUSER REQUIREMENTS FOR HIGH EXPANSION RATIO SPACE ENGINE

FINAL REPORT

November 1981

Contract NAS8-33981

Prepared for National Aeronautics and Space Administration
Marshall Space Flight Center, Alabama 35812

by

C. J. Wojciechowski
P. G. Anderson

APPROVED: C. Donald Andrews

C. Donald Andrews, Manager
Systems Analysis & Simulation Section

George D. Reny

George D. Reny
Director

FOREWORD

This report presents the analytical results of a study to define the diffuser requirements for sea level testing of high expansion ratio space engines. The work was performed by personnel in the Systems Analysis & Simulation Section of the Lockheed-Huntsville Research & Engineering Center under NASA contract NAS8-33981. The NASA Contracting Officer's Representative for this study was Mr. K. E. Riggs, EP23.

CONTENTS

CONTENTS (Cont'd)

1. INTRODUCTION

The design of a supersonic diffuser which will be compatible with a family of space engine systems and sea level test conditions is a complex task.

Lockheed-Huntsville has previously performed preliminary analyses of the diffuser requirements for sea level testing of the space engines, i.e., the staged combustion and expander cycle engines. In the previous studies (Refs. 1 and 2) specific diffuser designs were evolved. Since it was a design goal of MSFC to construct a "building block" space engine diffuser in which a whole series of space engines could be tested (for use on the Orbiter Transfer Vehicle) this study effort was initiated.

The study effort had three objectives:

1. Review and update the analytical techniques used in diffuser design.
2. Select the best of the analytical methods and conduct a parametric analysis of diffuser requirements.
3. Apply the analytical techniques to a specific diffuser requirement.

Diffuser starting transients and associated phenomena become more critical as the nozzle area ratio is increased or the chamber pressure reduced. In fact, under the above conditions the diffuser start transients can either make or break a diffuser design. It is fundamentally important to a successful diffuser design to thoroughly understand a particular diffuser starting phenomenon. The results of the analysis will also lead to operational sequences which must be performed. The "state of the art" of diffuser design

will be steadily pushed forward by the proposed MSFC Diffuser Facility and in many cases, the data will not exist in the literature. Therefore, extrapolations of existing data using sound and fundamental engineering theory as a basis will be necessary. Another important consideration for performing this analysis is the effect the physical presence of the diffuser will exert on the engine during the start transients. Ideally, the diffuser should simulate the space vacuum environment. The physical presence of a diffuser, however, will alter the engine starting phenomena due to shock reflections, and start transient measurements may not be representative of a space vacuum start.

2. TECHNICAL DISCUSSION

2.1 LITERATURE REVIEW

Research effort has been directed in the past (Refs. 1 through 25) toward development of analytical methods for determining the performance of nozzle-diffuser systems. Analytical methods are avialable but are generally limited to the engine nozzle and entrance portion of the diffuser up to the second throat. In addition, empirical procedures have been developed which appear to be valid for predicting base pressure, overall diffuser performance and starting pressure ratio. The many factors not incorporated into the empirical methods prevent a purely theoretical approach to the diffuser design. Hence, past diffuser test experience is an important factor in designing a new diffuser system. Some of the factors not considered in the empirical methods are:

1. Heat transfer effects
2. Initial boundary layer effects
3. Real gas variable gamma effects
4. Non-isoenergetic mixing effects
5. Nonuniform flow fields downstream of the nozzle throat including regions of supersonic flow with bifurcated shocks and regions of subsonic flow.

Hence the present "state of the art" for design and analysis of nozzle-diffuser systems consists of two basic procedures:

1. Empirical Methods: These methods involve calculations using available compressible flow equations using isentropic, adiabatic and normal shock relations corrected by empirical factors which have been obtained experimentally for a variety of configurations.

2. Theoretical Methods: These methods utilize the computer to analyze the nozzle and diffuser flowfield and are capable of treating one or more of the factors listed above which the empirical methods do not consider.

2.2 DEVELOPMENT OF DIFFUSER DESIGN EMPIRICAL METHODS

The application of the empirical method used to design the engine diffuser is presented next.

The general theory based on the simultaneous solution of the continuity, impulse, energy and state equations is presented in Ref. 3. The space engine parameters are presented in Table 3-1. As will be mentioned in section 3, the effective ratio of specific heats, γ, for these engines is 1.22. This value will be used throughout this analysis. In order to reduce the diffuser entrance Mach number the diffuser entrance diameter is not made any larger than is absoutely necessary. Therefore the diffuser entrance diameter is generally fixed at 0.5 in. larger than the nozzle exit cutside diameter. The simultaneous solution of the continuity, impulse, energy and state equations results in an expression which may be expressed graphically as a function of γ with Mach number as a parameter. This expression is:

$$\frac{\dot{m}}{\Sigma F}\sqrt{\frac{RT_t}{g_c}} = \frac{M\sqrt{\gamma}\sqrt{1 + \frac{\gamma-1}{2}M^2}}{1 + \gamma M^2}$$

where

$\dot{m}$ = propellant mass flow rate in lbm/sec

ΣF = reaction force in lbf

R = gas constant in ft-lbf/lbm R

T_t = total temperature in R

g_c = gravitational constant in lbm-ft/lbf-sec^2

M = Mach number

γ = ratio of specific heats

A graph of this parameter is presented in Fig. 2-1.

Straight Diffuser Analysis

A sketch of this diffuser is shown in Fig. 2-2. The step-by-step analysis follows.

The diffuser entrance area to engine throat area ratio is

$$A_D/A_n^* = A_e/A_n^* \times A_D/A_e.$$

Using this area ratio, the diffuser entrance Mach No. (M_D) is obtained from isentropic tables at $\gamma = 1.22$

then from isentropic tables look up

P_e/P_t, normal shock Pt_2/Pt_1 and normal shock P_2/P_1, and

calculate the diffuser entrance force using the general thrust equation:

$$F = P_1 A_D(1 + \gamma M^2).$$

Based on equilibrium chemistry data, the total temperature at the nozzle exit is obtained. Now compute the expression:

$$\frac{\dot{m}}{F}\sqrt{\frac{RT_t}{g_c}}$$

Using this parameter in conjunction with Fig. 2-1 and assuming the diffuser L/D is approximately 8 or more, the exit Mach number is calculated.

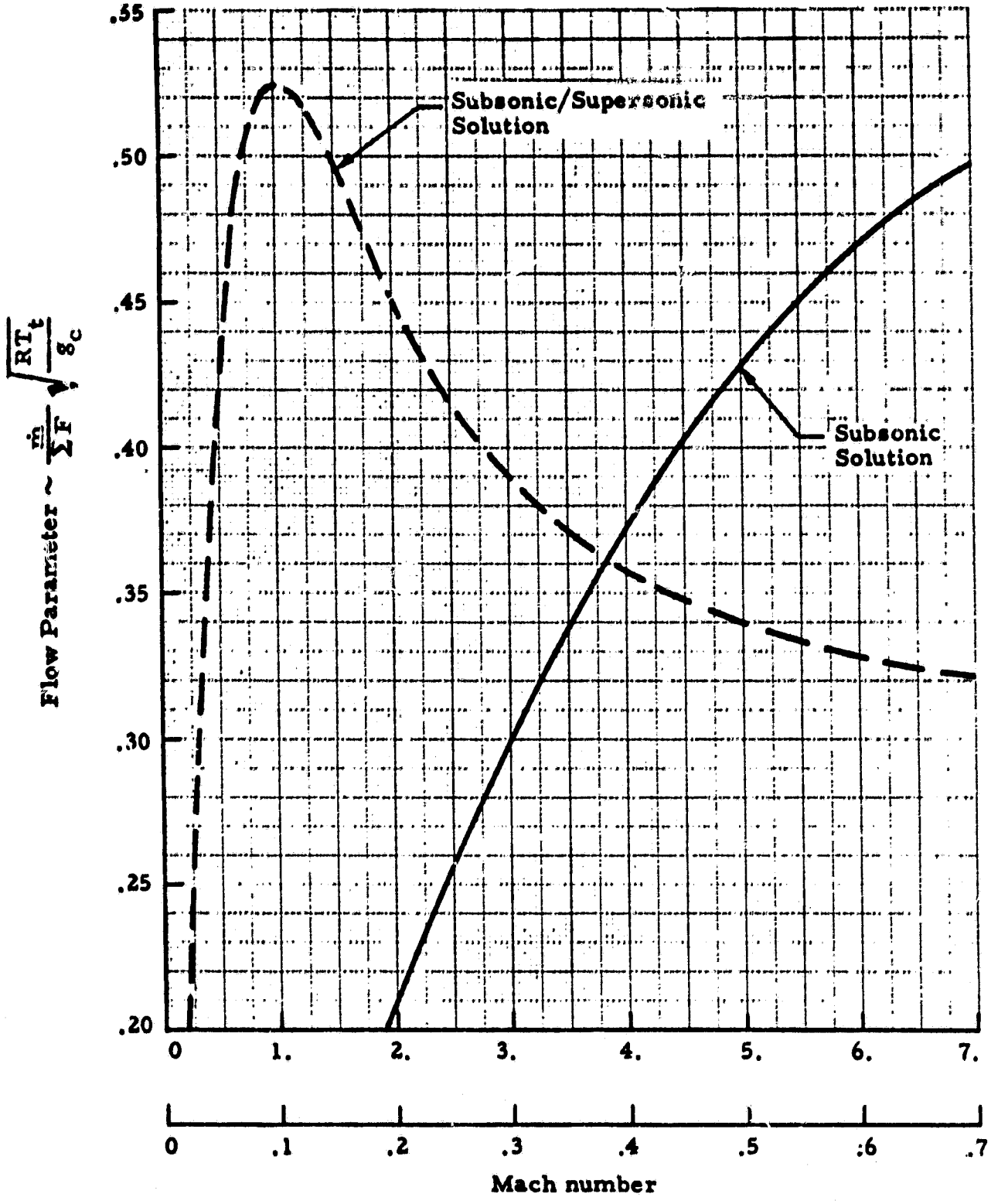

Fig. 2-1 - Graphical Solution for Flow Parameter versus Mach Number, $\gamma = 1.22$

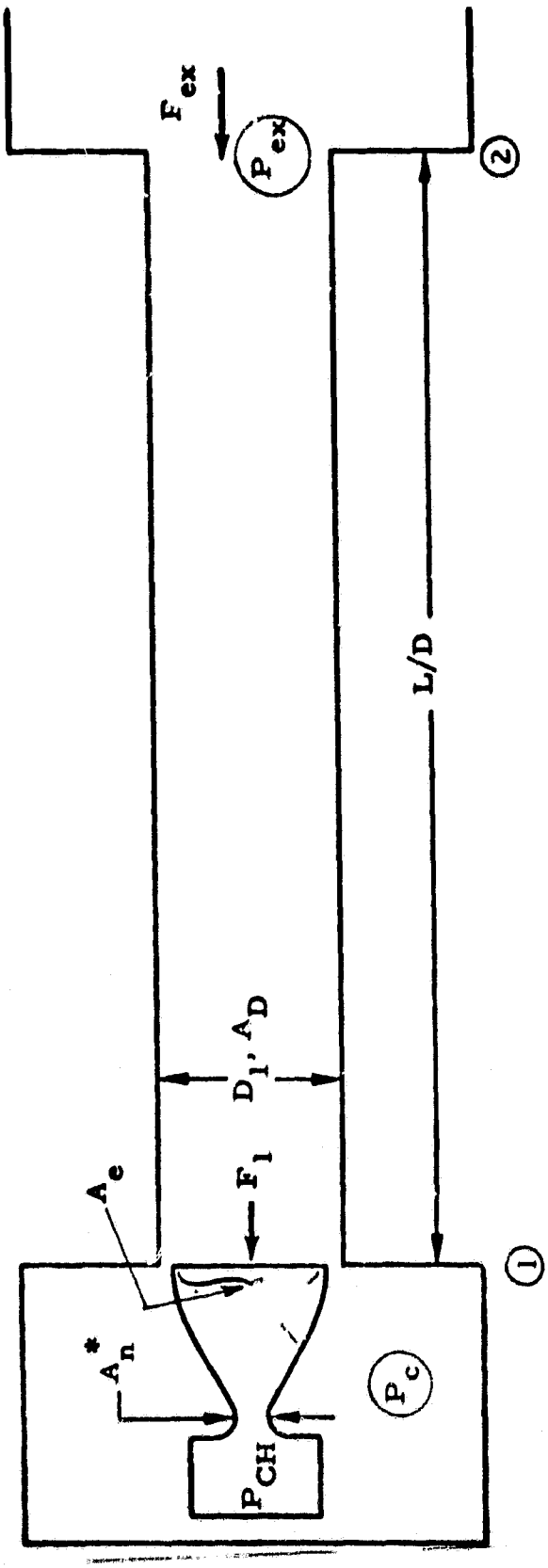

Fig. 2-2 - Sketch of Straight Duct Diffuser Characteristics

Neglecting wall friction, and heat transfer, the general thrust equation can be used to predict the diffuser exit pressure, P_{ex}:

$$P_{ex} = \frac{F}{A_D\ (1 + \gamma\ M_{ex}^2)}$$

As a check on this exit pressure we can use the normal shock pressure rise and compute P_{ex} as

$$P_{ex} = P_2/P_1 \times P_1/P_{t_1} \times P_{CH}.$$

The value of P_{ex} calculated by this method agrees favorably with the previously calculated value. The diffuser starting pressure would be calculated as

$$P_{CH\ start} = 1.1 \times P_{CH}\ (14.7/P_{ex}).$$

Second Throat Diffuser Analysis

The area contraction ratio is based on normal shock theory. The diffuser contraction ratio is computed thusly;

$$\frac{A_D}{A_{ST}} = \frac{A_D}{A^*} \times \frac{P_{t_2}}{P_{t_1}}$$

$$\therefore A_{ST} = A_D \times A_{ST}/A_D$$

$$D_{ST} = \sqrt{\frac{4 \times A_{ST}}{\pi}}$$

In this case, the exit force (see Fig. 2-3) is determined as

$$F_{ex} = F_1 - F_{R_1} - F_{R_2}$$

in the absence of friction and heat transfer effects. Before we can proceed with the analysis further, a specific diffuser design must be established so that the forces acting on the two ramps can be calculated. In this study ramp angles were varied between 5 and 23 deg and flow properties were computed. The second ramp was added to increase the number of oblique shocks and therefore increase the diffuser efficiency (Refs. 4 and 8). For this design the resulting exit force is computed as:

$$F_{ex} = F_1 - F_{R_1} - F_{R_2}$$

$$= F_1 - P_{R_1} \pi/4 \ (D_1^2 - D_S^2) - P_{R_2} \pi/4 \ (D_S^2 - D_{St}^2)$$

The flow parameter is then calculated, i.e.,

$$\frac{\dot{m}}{F_{ex}} \sqrt{\frac{RT_t}{g_c}}$$

From Fig. 2-1, the exit Mach number is read and the exit pressure is computed as

$$P_{ex} = \frac{F_{ex}}{A_{ex} \ (1 + \gamma \ M_{ex}^2)}$$

Now assuming a 60% subsonic diffuser efficiency at M_{ex} the exit pressure, P_{ex} can be computed.

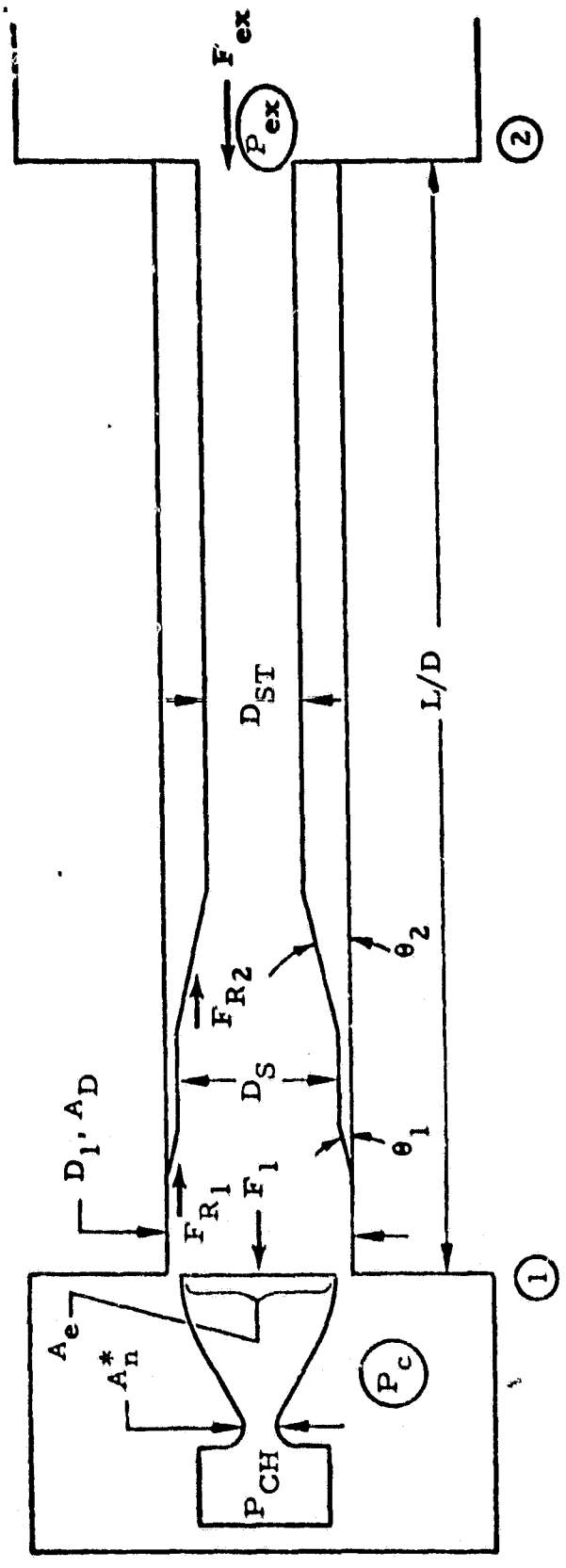

Fig. 2-3 - Sketch of Double Ramp Second Throat Diffuser Characteristics

The diffuser starting pressure is then calculated as before, i.e.,

$$P_{CH\ Start} = 1.1 \times P_{CH} \times 14.7/P_{ex}.$$

The diffuser second throat contraction ratio can also be obtained from experimental data as shown in Fig. 2-4. As shown in Fig. 2-4, experimental data indicate that for a properly designed second throat diffuser, the contraction ratio can be greater than one-dimensional normal shock theory suggests. The experimental curve will be used in the parametric analysis.

Ejector Analysis

An ejector is required when the diffuser exit total pressure is below 16.17 psia (assuming 10% margin). The ejector must be designed to meet the requirements of ignition, full power and steady state performance at 10% power level. Ejector performance is enhanced when the ejector exit static pressure matches that of the engine flow at the diffuser second throat exit (Refs. 16, 20, 24 and 25). In addition, ejector performance is further enhanced when the ejector flow expands radially outward (Ref. 16). The above statements infer that with fixed ejector flow rates, the ejector area ratio must be designed to be variable in order to match exit pressures at 10% and full power engine operation. In order to produce low cell pressures for ignition, a two-stage ejector is required with the first stage operating at a low flow rate (Fig. 3-4) and moderate Mach number.

The ejector performance analysis method as outlined in Ref. 25 was used in all the parameter analysis work which will be discussed in Section 3. The second stage ejector was required to allow the first stage ejector to flow when the engine flow was not present, i.e., during start up and shut down. The philosophy used in the ejector analysis was based on the following:

1. Analyses were conducted at the ejector exit and fully mixed stations without regard as to what transpired between (Ref. 24).

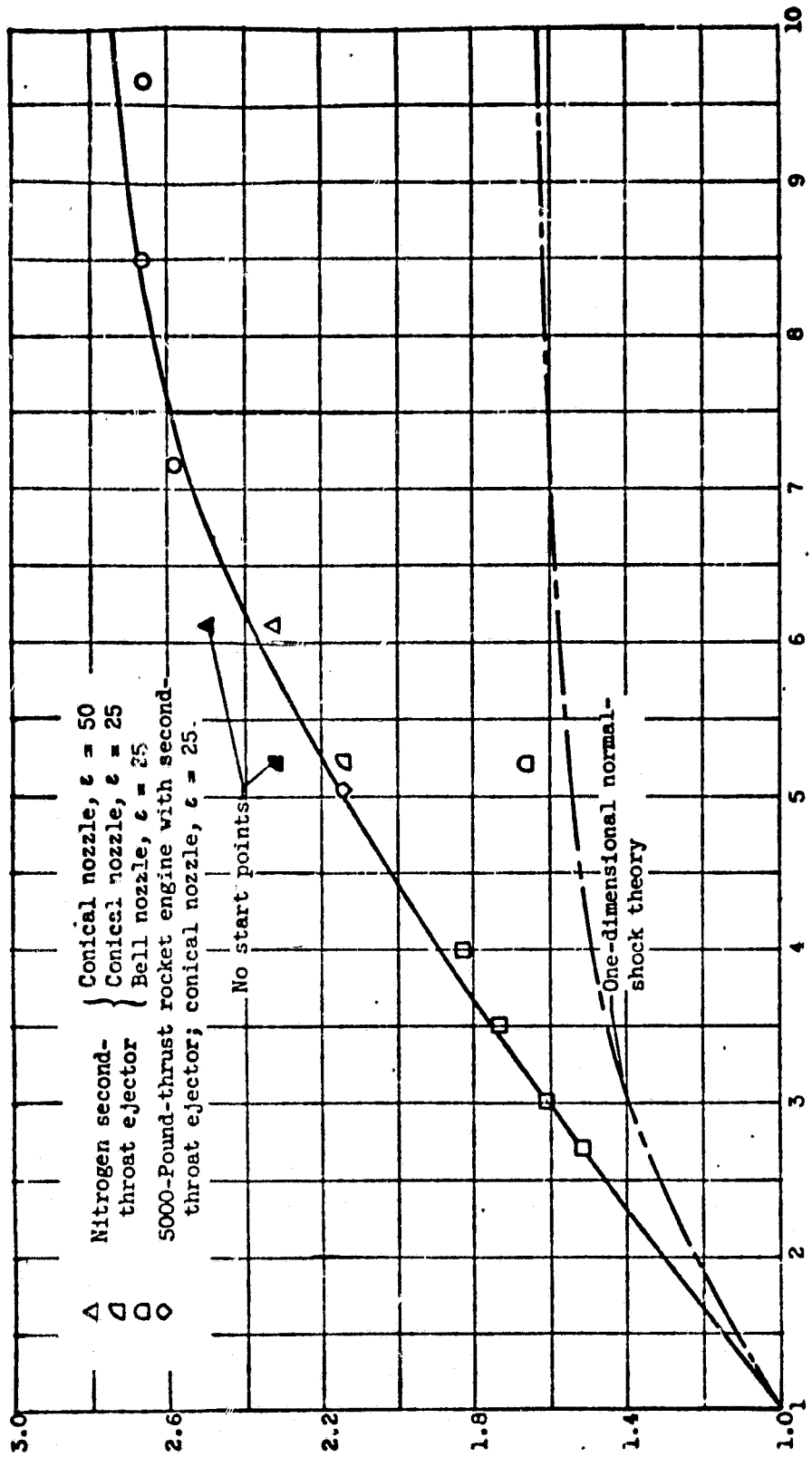

Fig. 2-4 - Effect of Diffuser Inlet Mach Number on Maximum Contraction Ratio for Starting. (Ref. 13)

2. Primary and secondary flow are fixed to have the same static pressure at the inlet to the mixing section.

3. Constant pressure mixing is assumed with subsequent flow area reduction down to the fully mixed region.

4. The flow conditions before and after mixing are related to each other by the conservation requirements for mass, momentum and energy.

5. Ejector length dimensions are based on available data to insure fully mixed conditions.

6. One-dimensional flow conditions with empirical corrections are assumed.

The ejector analysis method outlined above allows one to relate the ejector performance specified by ejector pressure ratio, and ejector to engine mass flow ratio to the mixing section geometry given by its principal cross-sectional areas.

2.3 DEVELOPMENT OF DIFFUSER DESIGN THEORETICAL METHODS

The General Interpolants Method (GIM) code (Ref. 27) was used to perform the Navier-Stokes analysis of the diffuser flow field. A brief summary of the code follows.

The GIM code employs a new methodology for constructing numerical analogs of the partial differential equations of continuum mechanics. A general formulation is provided which permits classical finite element methods and many of the finite difference methods to be derived directly. The GIM approach is new in the sense that it combines the best features of finite element and finite difference methods. The technique allows complex geometries to be handled in the finite element manner and operates on the integral form of the conservation laws. Solutions can be generated implicitly with the finite element analogs or by explicit finite difference analogs, which do not require a reduction of large systems of linear algebraic equations (no matrix inverse). A quasi-variational procedure is used

to introduce boundary conditions into the method and to provide a natural assembly sequence for combining the element equations into the full domain equations. Attempts have been made in the literature to relate finite difference and finite element methods but have achieved limited success, and apparently no one other than Lockheed-Huntsville has used a combination of the two approaches in this unique fashion.

As is the case with all attempts to solve partial differential equations by numerical approximations, the domain of interest is first discretized by appropriate subdivision into an assemblage of interconnected finite elements. A mesh generation is used in the GIM approach -hich incorporates general curvilinear coordinates, stretching transformations and bivariate blending to produce an automated mesh/element generation. Shape functions, based on a set of generalized interpolants, are then chosen to describe the behavior over each element. We then proceed, as in the Method of Weighted Residuals by multiplying the descretized equations by a set of weight functions and integrating over the volume of the element. A quasi-variational procedure is then used to construct the assembled system of equations from the element equations, and to introduce boundary conditions into the method.

By choosing the weight functions equal to the shape functions, we reproduce the classical finite element nodal analogs. It is at this point that we introduce one of the important concepts of GIM: orthogonal weight/shape functions. By appropriately choosing the weight functions to be orthogonal to the shape functions, we can obtain explicit nodal analogs. Further, by a choice of arbitrary constants in the orthogonal weight functions, we can reproduce known finite difference nodal analogs, such as centered difference, upwind/downwind differences and the two-step MacCormak algorithm. As a result of this spatial discretization, we have reduced the partial differential equations to ordinary differential equations with "time" as the independent variable. Any forward marching algorithm such as Euler, Runge-Kutta or predictor-corrector can be used to advance the solution profiles in time.

The GIM formulation is not a Finite Element method in the classical sense. Rather finite difference methods are used exclusively but the equations are written in general orthogonal curvilinear coordinates. Transformations are used to transform the physical planes into regions of unit cubes. The mesh is generated on this unit cube and the local metric coefficients generated. Each region of the flow domain is likewise transformed and then blended to form the full flow domain. In order to treat completely arbitrary geometric domains, different transformations may be employed in different regions. For this reason, we then transform the blended domain back to physical space. This allows the same set of equations to be solved in each region, with the local Jacobian of the transformation being the coefficients.

This is not the classical treatment of many finite difference codes. To compute on the unit cube itself, one single transformation would be required for the entire domain. This would restrict the type of geometries that could be modeled.

The following discussion summarizes each module of the code. The GIM code is divided into four modules: (1) mesh generation/geometry; (2) nodal analog/matrix assembly; (3) unsteady integration; and (4) graphics. The mesh generation module accepts boundary geometry data, curve or line formula flags, and number of cuts in each coordinate direction. A set of general curvilinear maps is then used to subdivide each region into finite elements. Each region which is input is processed and then blended together. The output is a set of coordinates for each element along with the element coefficient matrices. The nodal analog assembly module takes the mesh data from a stored external file and performs via quasi-variational procedure, the assembly of the element equations into the full domain equations. At this point, the dynamic storage allocation is set up so that the unsteady integration module can integrate with virtually unlimited problem size.

The unsteady integration module performs the actual computation of the flow by employing the boundary conditions selected by the user. The nodal analog at this point is arbitrary and any one of a number of schemes can be

selected depending on the problem being analyzed. The solution is marched forward in time for a specified number of steps or until a steady state is reached. The data display module reads the solution profiles from external storage (drum, tape) and prints, plots and maps the flow parameters. Fig. 2-5 below is a block diagram illustrating the modular construction of the GIM code.

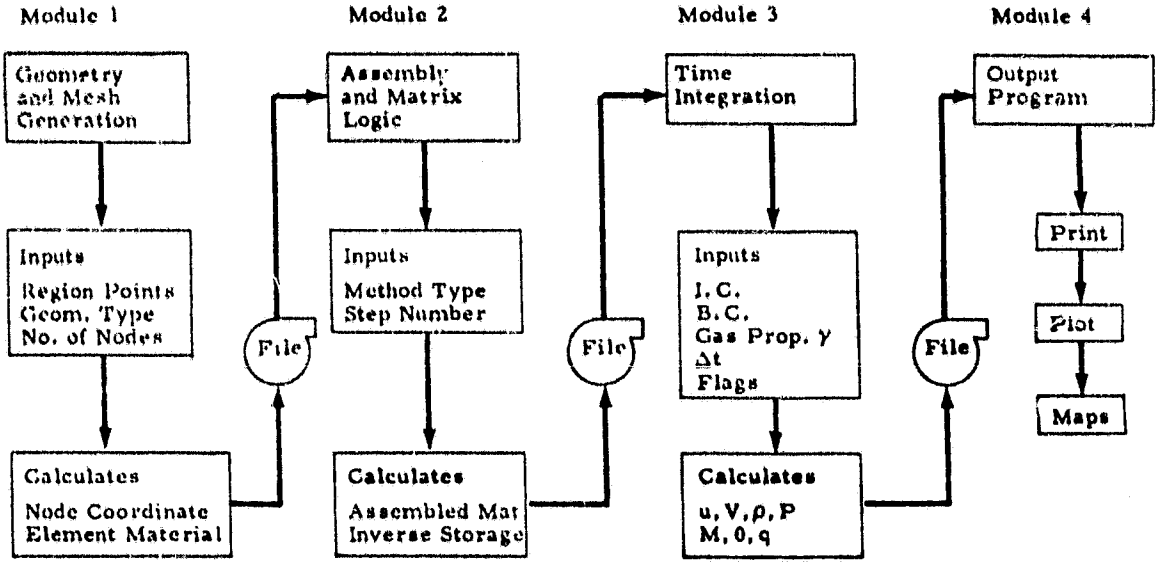

Fig. 2-5 - GIM Code Block Diagram

The current version of the code can compute axisymmetric, and two- and three-dimensional viscous flows of an ideal gas in arbitrary geometric domains. The unsteady integration module is coded such that additional capability can be readily adapted such as different equation sets, other boundary values, virtually unlimited nodal points and time marching schemes.

Through the choice of the arbitrary constants in the orthogonal weight functions a forward-marching, or "quasi-parabolic" (QP) algorithm can be employed in the GIM code. The forward marching technique requires only two computational planes to be in the computer at one time instead of the entire flow field. This reduced storage greatly reduces computer runtime and is therefore advantageous for supersonic flows.

The diffuser flow field was modeled for the GIM code on the CDC CYBER 203 computer at Langley Research Center. The entire flow field was modeled using the forward marching or QP algorithm. The QP solution resulted in a completely supersonic flow field with no normal shock in the tubular section. The results of the QP analysis at the entrance to the tubular section was to be input into a GIM code elliptic solution to compute the normal shock resulting from increased exit pressures. This elliptic solution was not performed due to program effort redirection by NASA/MSFC.

3. PARAMETRIC ANALYSIS OF DIFFUSER REQUIREMENTS

In this section of the study, a parametric analysis was conducted using nozzle area ratio, ε, chamber pressure, P_c, and degree of ejector flow augmentation, $\dot{m}_{Aug}$, as independent parameters. The diffuser configuration parameters, such as area contraction ratio, A_{ST}/A_D, length to diameter ratio, L/D, and the ejector design Mach number were design variables. At this time in the study, based on previous results (Refs. 1 and 2), it was decided to fix the ejector inlet total conditions to correspond closely to the conditions which exist at the turbine exit in a turbojet engine. The ejector inlets were thus fixed, but the mass flow to each ejector was varied as required. To accomplish this study the one-dimensional empirical methods presented in Section 2 of this report were programmed on the in-house PDP-11 digital computer. Then, using the results generated, diffuser commonality and "building block" approach was considered. In the above analysis, a 10% starting margin (based on chamber pressure) was used.

Table 3-1 presents the characteritistics of five candidate space engines. Since the "building block" diffuser must accommodate all of these engines, the diffuser duct inlet diameter D_D was set at 73.5 in.

The thermochemical properties for the LOX-LH_2 propellant system were obtained from Ref. 26 and previous chemical equilibrium combustion computer program runs made for similar operating conditions. The results of this data, indicate that the ratio of specific heats, γ, varies from 1.14 in the combustion chamber to 1.32 near the nozzle exit plane. It was determined that for use in the simplified one-dimensional flow diffuser analysis that an effective γ of 1.22 would yeild satisfactory nozzle exit flow conditions.

Table 3-1 - FIVE CANDIDATE SPACE ENGINES FOR THE OTV

Parameter	Units	AECE-A	AECE-P	AECE-R	ASE	RL10-I1B
Thrust, Full	lb	15000	15000	15000	2000	15000
Thrust, Low	lb	2000	1500	1800	1850	1500
Maximum Test Duration @ MR = 6.0						
Full Thrust	sec	1200	1200	1200	1200	1200
Low Thrust	sec	2500	2500	2500	2500	2500
Gimbal Capability	—	none	none	none	none	none
Propellants		LOX/LH_2	LOX/LH_2	LOX/LH_2	LOX/LH_2	LOX/LH_2
Mixture Ratio, Full Thrust	—	6.0	6.0	6.0	6.0	6.0
Low Thrust	—	6.0	6.0	4.0	2.0	6.0
Nozzle Area Ratio	—	473	642	625	400	205
Engine Evelope:						
Outside Diameter @ Noz. Exit	in.	62.7	66.1	63.25	58.08	73.0
Inside Diameter A Noz. Exit	in.	60.7	64.1	61.25	56.08	71.0
Length, Gimbal Pad to Noz. Exit	in.	120	114	117	100	110
Length, Gimbal Pad to Inlet Flange						
LOX	in.	12	12	12	27.1	10
LH_2	in.	15	15	15	36.87	10
Engine Weight	lb					
Chamber Pressure, Full Thrust	Psia	1200	1505	1539	2028	400
Cahmber Pressure, Low Thrust	Psia	160	150	198	187	40
Noz. Exit Wall Press., Full Thrust	Psia	0.196	0.163	0.172	0.406	0.19
Noz. Exit Wall Press., Low Thrust	Psia	0.026	0.016	0.022	0.037	0.019
Total Flow Pate, Full Thrust	lb/sec	31.4	31.2	31.2	42.01	32.6
Total Flow Rate, Low Thrust	lb/sec	4.2	3.2	3.7	4.06	3.2

No γ changes were considered in the analysis. Additional study effort should be undertaken to determine the effects of the real gas variable γ on the diffuser design. The ratio of specific heats used for tha ejector flow was $\gamma = 1.33$.

Basically two specific tasks were undertaken and the results are presented in each one.

3.1 PARAMETRIC ANALYSIS FOR AN UNAUGMENTED DIFFUSER

In this task, both high chamber pressure (high thrust) and low chamber pressure (low thrust) operation were analyzed as to the maximum allowable nozzle area ratio which tested in an unagumented diffuser. The results are presented in Figs. 3-1 and 3-2. Figure 3-1 presents the results for the low chamber pressure operation, and Fig. 3-2 presents the results for the higher chamber pressure operation. As shown in Fig. 3-2 only the ASE engine can be run in a properly designed unaugmented diffuser.

3.2 PARAMETRIC ANALYSIS FOR AN AUGMENTED DIFFUSER

For the performance of this task the original computer program developed to accomplish Task 3.1 was modified to analyze diffuser and ejector performance together and ejector performance alone with no engine flowing so that ejector blank off performance could be evaluated. The computer program has the capability to add up to two ejectors (working in stages) as required to make the engine diffuser combination flow against ambient pressure. A +10% margin on chamber pressure is incorporated into the diffuser design computer code (DIFEJJ).

For this task a decision had to be made on a choice of ejector fluid. As mentioned earlier in this section, turbojet exhaust was selected over steam. The reasons for this selection were:

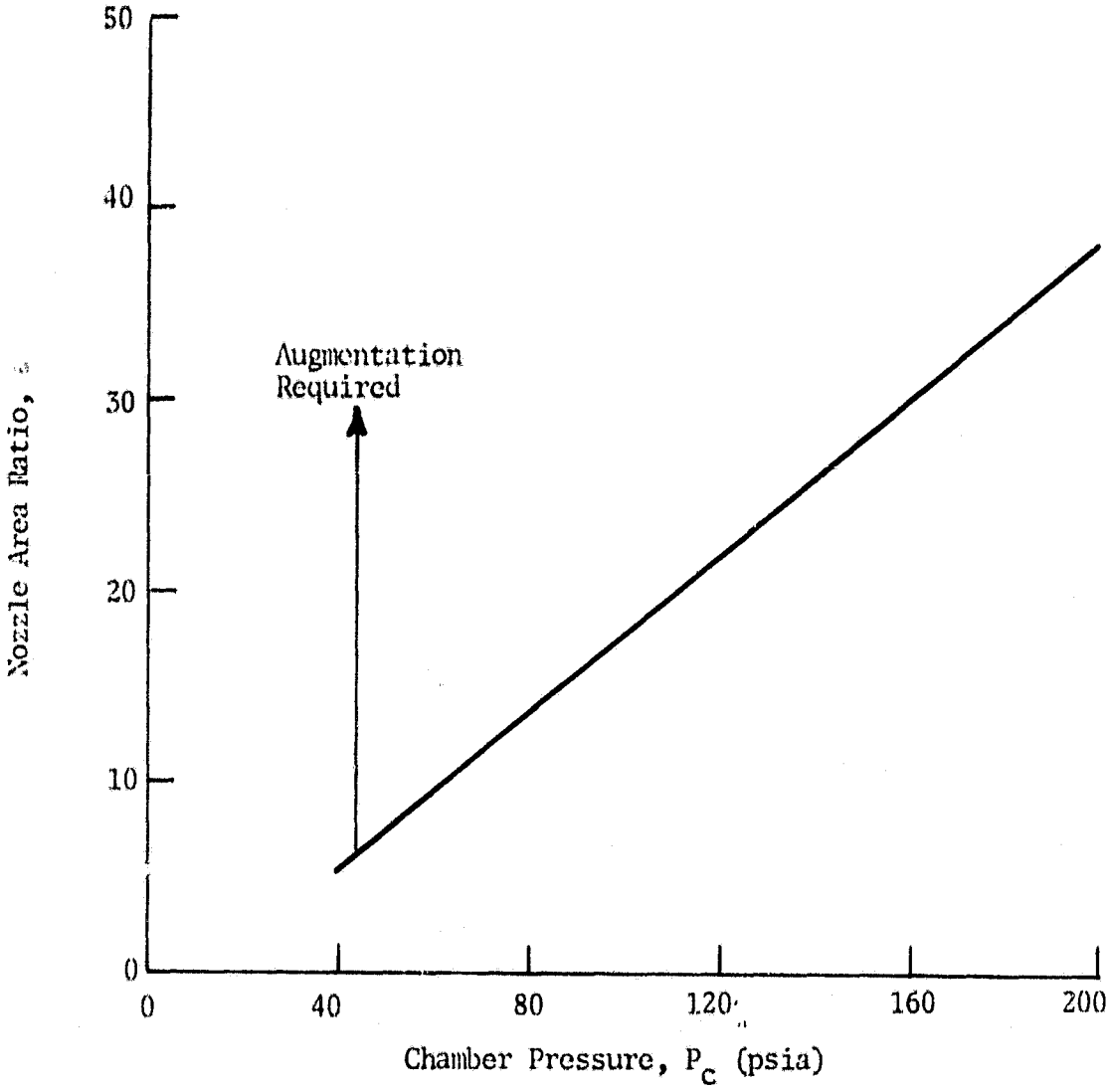

Fig. 3-1 - Unagumented Diffuser Limiting Area Ratios for Various Space Engine Chamber Pressures (Low Thrust)

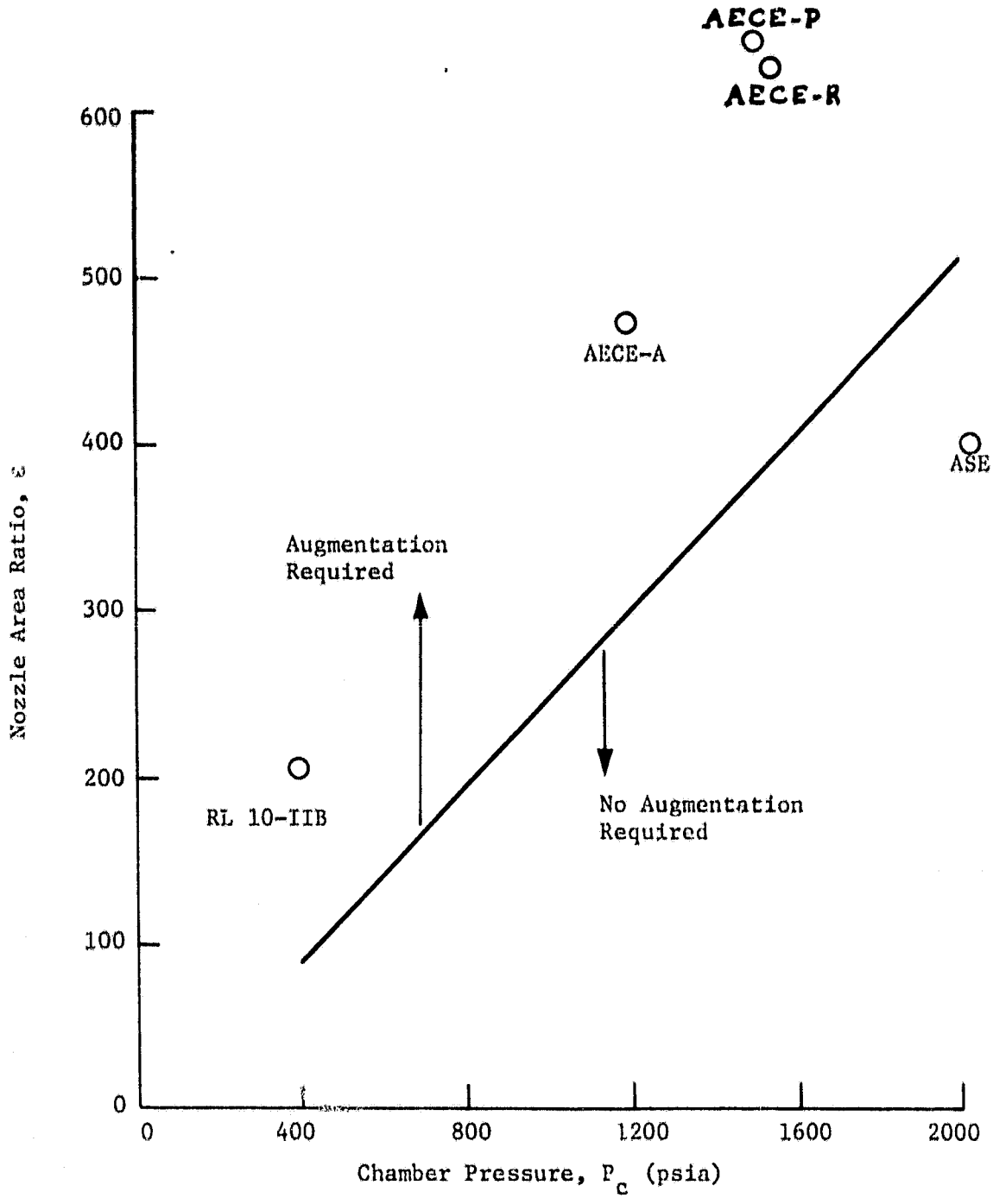

Fig. 3-2 - Unaugmented Diffuser Limiting Area Ratios for Various Space Engine Chamber Pressures (High Thrust)

1. Engine test durations of 30 min are required, consuming ejector fluid at a rate in excess of 300 lb/sec. An equivalent steam ejector system would require a building 100 ft by 300 ft by three stories high just for the steam generating equipment.

2. Quick startup capability using turbojets

3. More reliable operation than a steam system, and

4. Lower capital investment and much lower operating cost.

Turbojet engine literature was reviewed as to the exhaust flow properties. Typical turbine exist flow properties are presented in Fig. 3-3 which shows the "building block" diffuser and ejector configuration. One main requirement placed on the ejector system was that it be able to evacuate the diffuser down to at least 0.4 psia. Fig. 3-4 shows the typical variation of diffuser evacuation pressure with ejector flow rate for two different ejector design Mach numbers. As a result of studies like these it was decided to fix the ejector flow rates at 32.6 lbm/sec for ejector 1 and 293.4 lbm/sec for ejector 2. These flow rates correspond to several available turbojet engines such as the General Electric J85 and the Pratt & Whitney JT-11B-2 (J58).

The results of this parametric study are shown in Fig. 3-5. The results indicate that with a properly designed diffuser and two stage ejector system, space engines with area ratios up to 2000:1 and chamber pressures down to 40 psia can be tested. For all the envelope shown, the diffuser evacuation pressure was between 2.0 mmHg and 4.0 mmHg. The first ejector Mach number varied from 1.2 to 4.54. The second ejector Mach number varied from 2.44 to 2.66. The operation of the ejector/diffuser system is as follows:

1. The specific space engine is located on the operational envelope (Fig. 3-5) in terms of engine chamber pressure and area ratio. The space engine will fall in either one of three categories.

   - No augmentation required for space engine operation
   - First stage ejector required for space engine operation
   - Two-stage ejector required for operation.

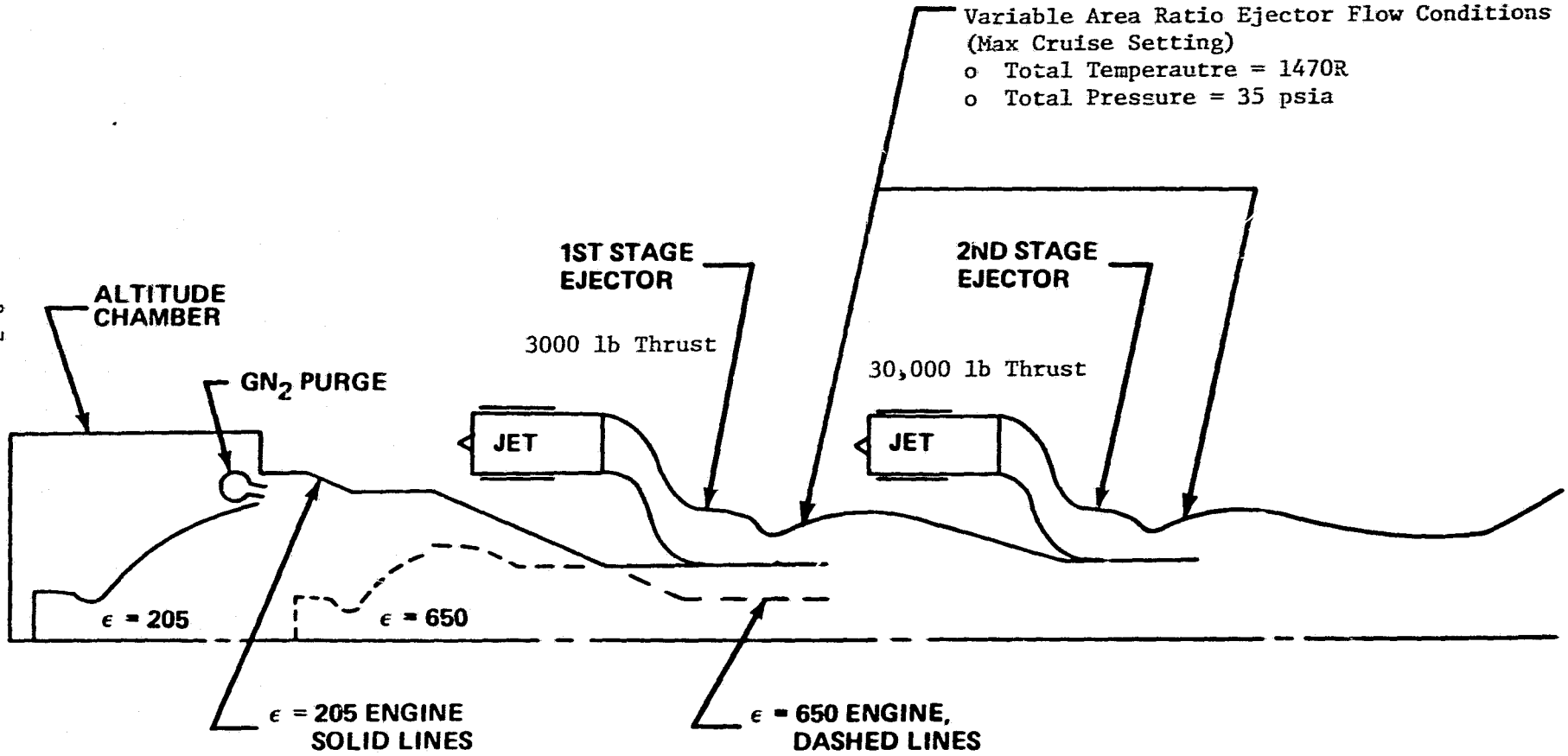

Fig. 3-3 Building Block Jet Engine Driven Ejector/Diffuser System

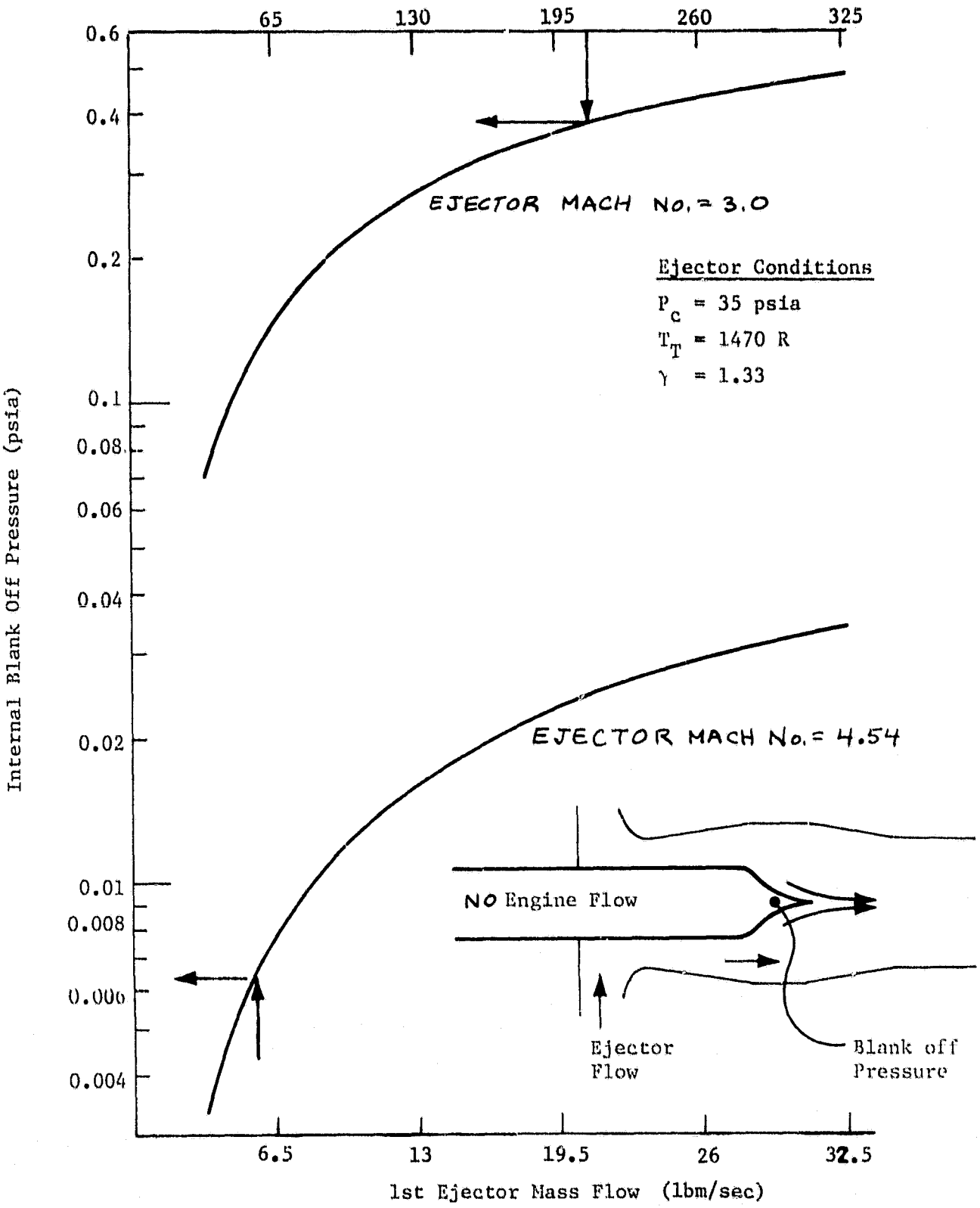

Fig. 3-4 - Diffuser Evacuation Pressure Versus Ejector Mass Flow

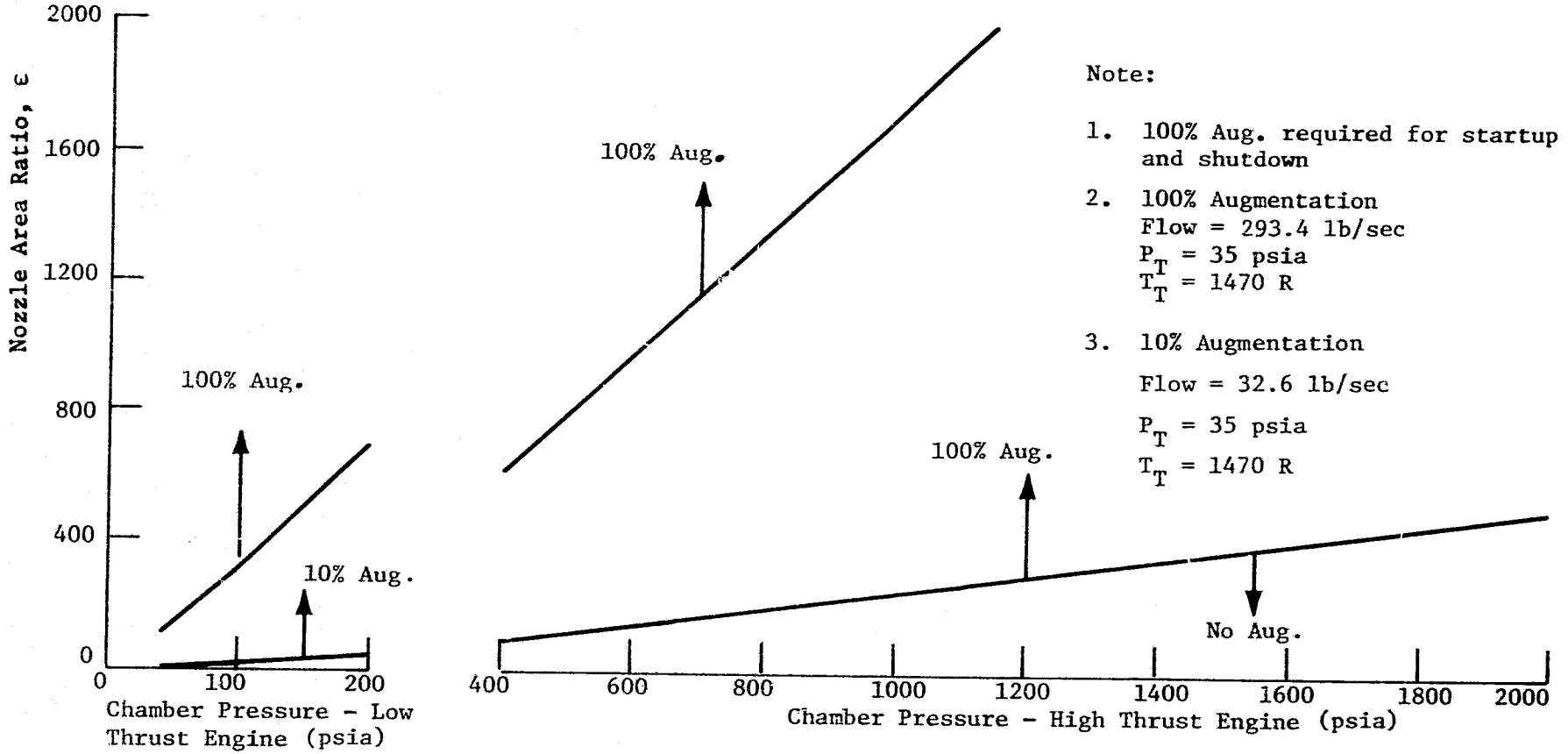

Fig. 3-5 - Diffuser/Ejector Operational Envelope in Terms of Space Engine Parameters

2. If the space engine requires only the first-stage ejector for operation, both stages must be used during start up and shut down. The system also features a gaseous nitrogen (GN_2) purge system as an extra safety precaution to eliminate the possibility of detonation on start up due to fuel lead. Prior to startup the two-stage ejector is designed to evacuate the diffuser down to 0.06 psia or 3 mmHg. An equivalent steam ejector system would require a three stage ejector system.

4. DIFFUSER REQUIREMENTS EXAMPLE

In this study, the general rocket exhaust diffuser requirements were investigated for the sea level testing of the RL10-IIB (Table 3-1) Pratt Whitney Expansion Cycle engine. The operating parameters for the engine are presented in Table 3-1. A preliminary engine exhaust diffuser design ws developed and is presented in this section. Detailed engine nozzle and diffuser flowfield analyses were performed. The RL10-IIB engine diffuser design was developed first since this engine will be available first and its diffuser operating data will be invaluable in establishing the diffuser requirements for the other space engines. The results obtained from this preliminary study are summarized in this section.

4.1 GEOMETRY DESIGN DETAILS

The diffuser design function must be performed before detailed flow analysis can be performed. In order to maintain the required low nozzle exit pressures for the nozzle to flow full, and still exhaust to atmospheric conditions, the supersonic diffuser must exhibit a pressure recovery better than normal shock recovery based on a cavity free stream Mach number of approximately 6. Based on a review of the literature, Ref. 1 through 25 and various LMSC reports this requirement necessitates the use of a specially designed second throat. The second throat minimum area is still based on the normal shock method since during starting, the second throat area must still be large enough to pass the normal shock flow. A range of second throat inlet ramp angles between 5 and 23 deg was investigated in this study. To obtain good total pressure recovery in as short a distance as possible, a double ramp second throat was selected (Ref. 4). This type of design was built and tested in the Ref. 4 study with excellent results. One interesting flow phenomena situation which occurred during this analysis and was borne out in the Ref. 4 tests, is the length of the cylindrical section between the first and second

ramps as shown in Fig. 4-1. The analysis indicated that if this cylindrical length is too long, the flow will expand back to a high Mach number with subsequently larger total pressure losses. This phenomenon was demonstrated in the Ref. 4 study when the diffuser starting pressures were reduced substantially when the length-to-diamter ratio of the cylindrical section was reduced from 1.53 to 0.51.

4.2 ONE-DIMENSIONAL ANALYSIS RESULTS

The overall diffuser design (Figs. 4-1 and 4-2) is based on the experimental and analytical results presented in Refs. 3 and 4 and discussed further in Section 2. The overall diffuser design was calcualted using the empirical one-dimensional diffuser/ejector design code (DIFEJJ) developed in this study.

The first stage ejector exit conditions shown in Figure 4-3 for this design are as follows, i.e.,

- High Thrust operation (Pc = 400 psia)

  Ejector Mach number = 1.72
  Blank-off pressure = 0.068 psia
  Flow Rate = 32.6 lbm/sec

- Low Thrust operation (Pc = 40 psia)

  Ejector Mach number = 3.15
  Blank-off pressure = 0.055 psia
  Flow rate = 32.6 lbm/sec

  } Not shown in Fig. 4-3

The second stage ejector operating conditions are shown in Fig. 4-4. The second stage ejector Mach number for the high thrust and low thrust operation are 2.52 and 2.39, respectively. The high thrust operation variables are presented in Figs. 4-3 and 4-4.

The high thrust mode of operation will impose the most severe heat loads, therefore the flowfield details were developed for it.

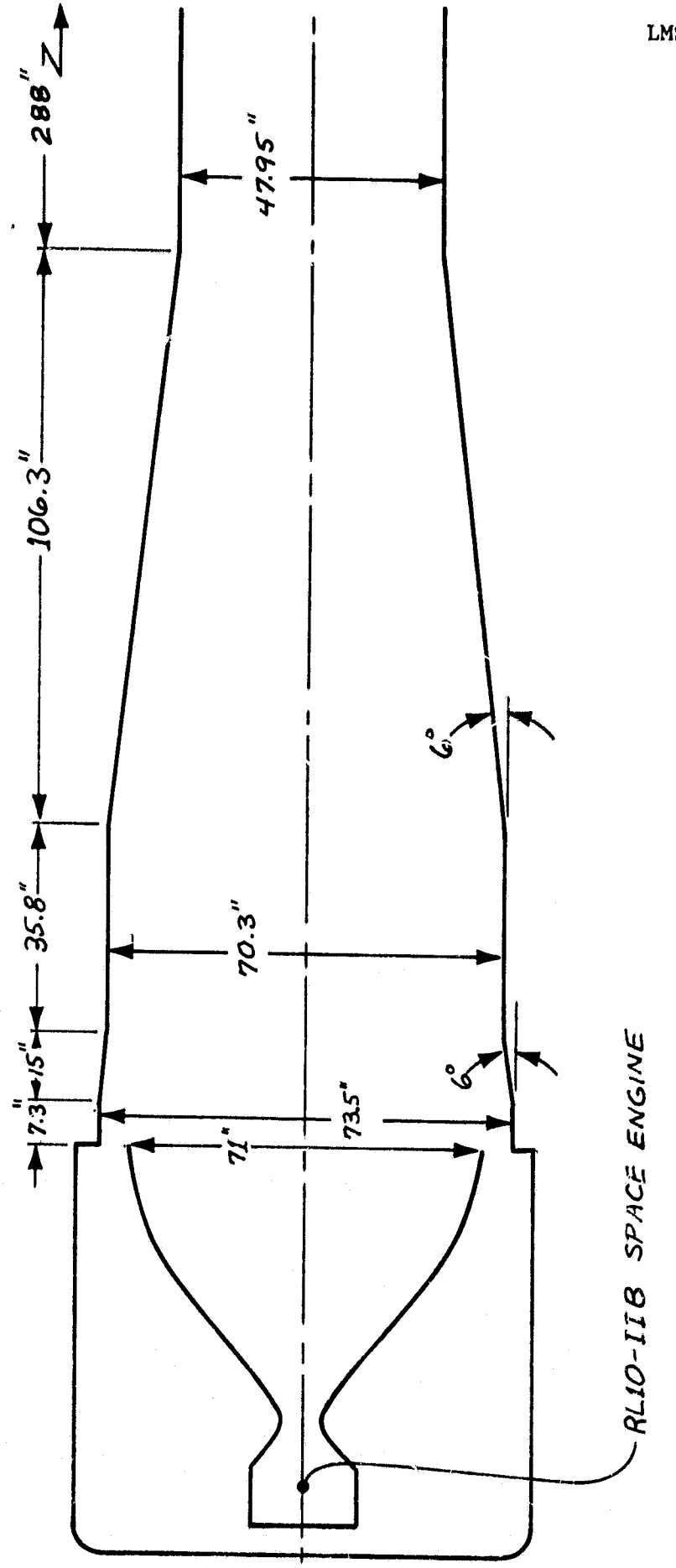

Fig. 4-1 - Diffuser Design for the RL10-IIB Space Engine

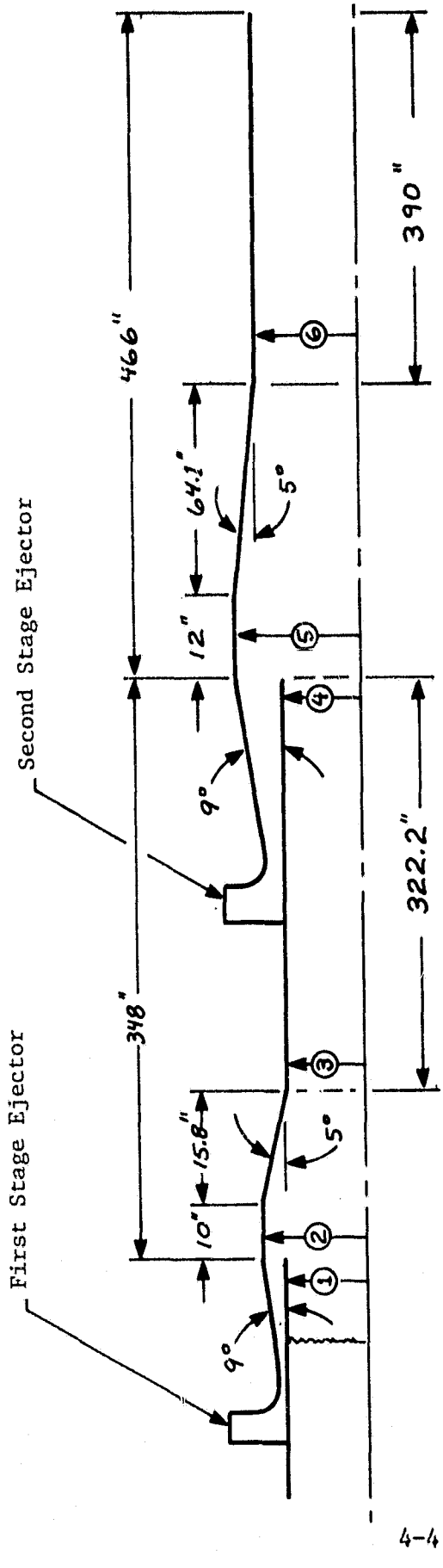

D_1 = 48.53"
D_2 = 49.7 "
$D_3 = D_4$ = 46.93"
D_5 = 66.5"
D_6 = 55.28"

Fig. 4-2 Two Stage Ejector System Design for the RL10-IIB Engine Diffuser

1-D Empirical Results (DIFEJJ Code)

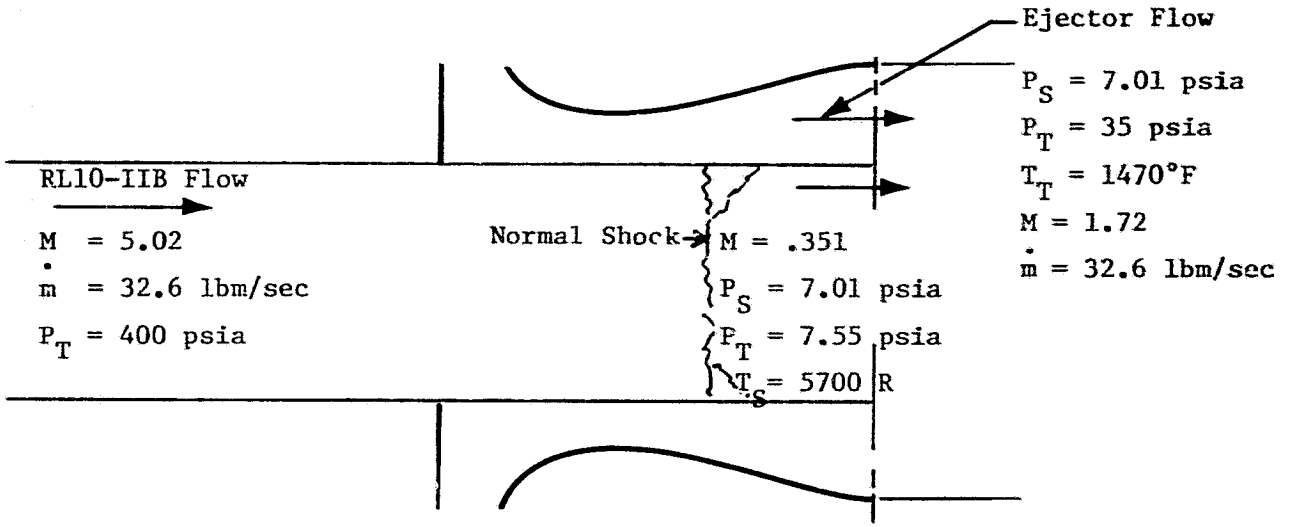

Axisymmetric GIM Code Parabolic Solution Results

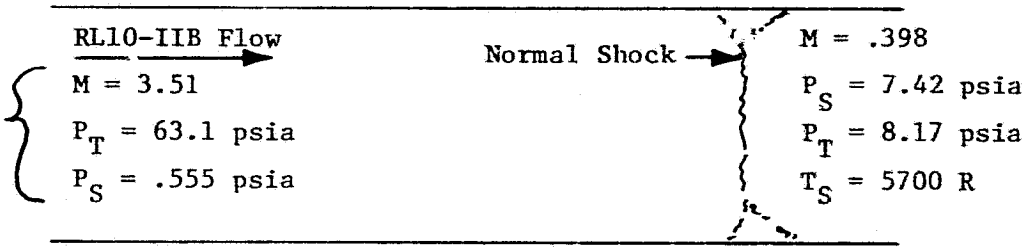

Cross section averaged properties

Fig. 4-3 - First Stage Ejector Flow Conditions and Comparison of 1-D Empirical with Axisymmetric GIM Code Results

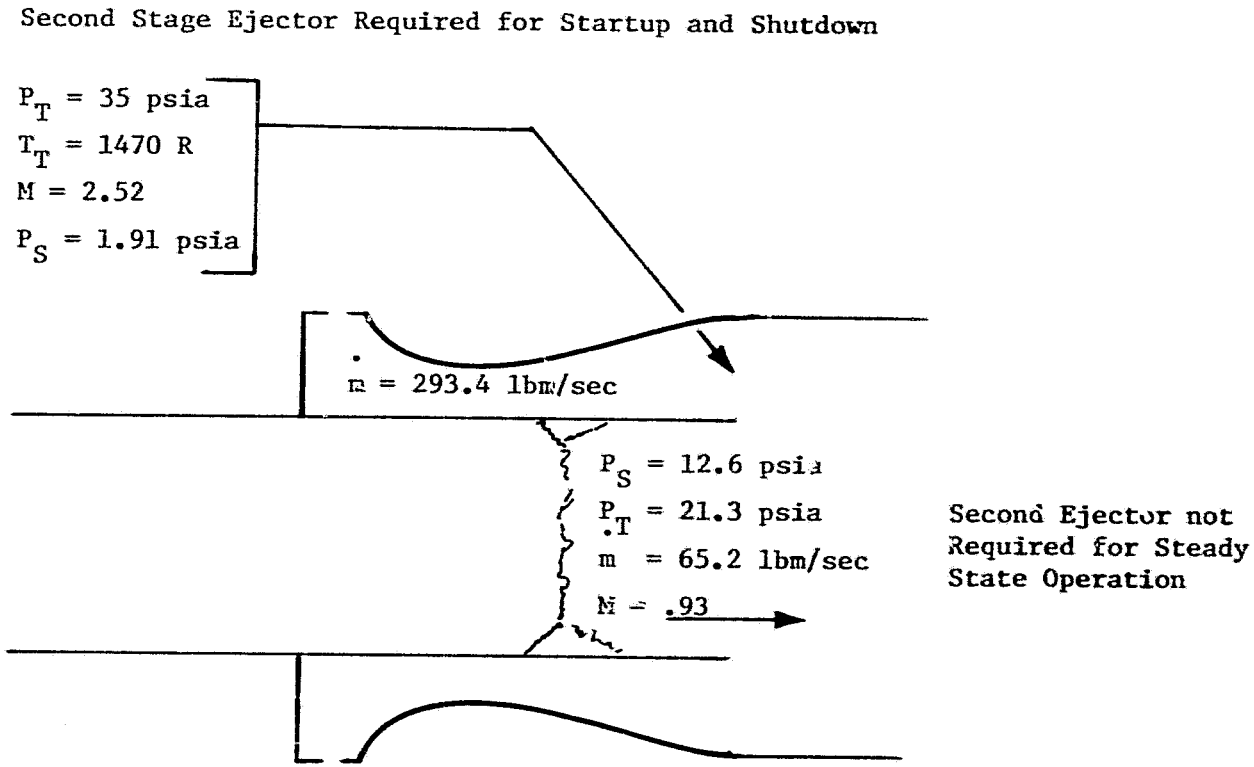

Fig. 4-4 - Second Stage Ejector Flow Conditions

4.3 DETAILED ANALYSIS RESULTS

In this section the results of the detailed analysis for the diffuser presented in Figs. 4-1 through 4-4 are presented. The results presented are for the flowfield parameters, heat loads, water cooling requirements, afterburning in the ejector mixing section and startup transient concerns.

4.3.1 Flow Field

The diffuser flow field was computed using the GIM code, discussed in Section 2.3, in the axisymmetric forward-marching mode. The geometry used in the analysis is shown in Fig. 4-5. The geometry was initiated downstream of the nozzle throat in order to ensure supersonic flow throughout the flow field. The nozzle was included in the analysis in order to obtain a good flow profile at the nozzle exit. The nozzle throat area used to compute the start line conditons was adjusted to accommodate the constant gamma assumption (γ = 1.22). Chamber conditions of 400 psia pressure and 5800 R temperature were used to compute the start line conditions along with a fluid flow rate of 32.6 lbm/sec and a mixture ratio of 6.0. The nozzle configuration was obtained from Pratt & Whitney through NASA-MSFC.

The diffuser geometry consisted of 364 planes containing 25 nodes each for a total of 9100 nodes. A free-slip tangency boundary condition was imposed on the diffuser wall. If the elliptic analysis of the tubular section had been performed, no-slip boundary conditions would have been imposed in order to develop the boundary layer in the tube.

Pressure contours for the resultant flowfield analysis are shown in Fig. 4-6. The pressure contours are not normalized (P_o = 1.0) and represent pressures in psfa. The wavy contours near the nozzle axis are due to plotter discretization and depict regions of nearly constant pressure. A strong oblique shock is generated when the nozzle flow encounters the diffuser wall. A second shock occurs when the diffuser necks down at a 6. deg angle. This second shock blends with the first as they reach the axis. A third weak oblique shock is generated at the second 6 deg ramp.

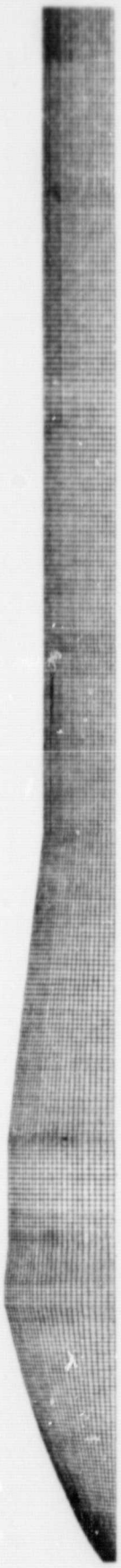

Fig. 4-5 - Diffuser Flowfield Geometry

Fig. 4-6 - Diffuser Flowfield Pressure Contours

The interaction of these shocks and their respected reflected shocks, along with the compression on the six-degree ramp, creates a very complex flow pattern just prior to entering the tubular section. The stronger reflected shock continues into the tubular section with decreasing strength.

The flow conditions along the diffuser wall, required for heat transfer analysis, are presented in Table 4-1.

4.3.2 Diffuser Heat Load Analysis

Heating rates to the inside wall of the diffuser were calculated using the Lockheed Multiple Pressure Gradient Program of Ref. 28. All heating rate calculations were based on the 100% thrust flow field assuming fully turbulent flow. The governing equations for the analysis are presented in Appendix A and were extracted from Ref. 28 for the convenience of the reader.

Thermal and transport properties used by the program are calculated using a model based on the Lennard-Jones potential intermolecular force model as documented in Ref. 28. The mass-fractions of the chemical species used in the analyses were determined using the NASA-Lewis CEC program. Chemical equilibrium was assumed at all locations. Chemical species considered in the heating analyses include H, H_2, HO_2, H_2O, O, OH, O_2. Heating rates based on a cold wall (540 R) are shown on Fig. 4-7 as a function of axial distance along the length of the diffuser. A peak in the heating occurs at a point just downstream of the point where the flow first impinges on the diffuser wall. The maximum heating value is approximately 87 Btu/ft^2-sec which occurs in the psuedo-shock flow region of the second throat tubular section. The change in slope of the heating versus distance curve at appoximately 22 in. is due to the flow expansion caused by the diffuser geometry changing from a conical to a cylindrical section.

Figure 4-8 shows the gas temperature, Fig. 4-9 shows the gas pressure, and Fig. 4-10 shows the gas Mach number along the diffuser wall.

Table 4-1 - DIFFUSER WALL CONDITIONS (Pc = 400)

X (ft)	R_{wall} (ft)	Density (lbm/ft^3)	Static Press. (psfa)	Mach No.
0.4814	3.0620	0.000194	39.760	4.405
0.5835	3.0620	0.000226	48.890	4.257
0.6856	3.0620	0.000256	57.660	4.146
0.7877	3.0620	0.000282	65.340	4.064
0.8878	3.0620	0.000303	71.760	4.011
0.9918	3.0620	0.000318	76.850	3.953
1.0940	3.0620	0.000352	89.070	3.807
(First Ramp)				
1.1850	3.0530	0.000383	99.180	3.744
1.2750	3.0430	0.000411	108.480	3.691
1.3660	3.0340	0.000434	116.160	3.650
1.4560	3.0240	0.000451	122.030	3.618
1.5470	3.0150	0.000462	126.010	3.595
1.6380	3.0050	0.000466	128.150	3.579
1.7280	2.9960	0.000466	128.530	3.520
1.8190	2.9860	0.000461	127.330	3.568
1.9090	2.9770	0.000452	124.760	3.572
2.0000	2.9670	0.000440	121.090	3.581
2.0910	2.9580	0.000425	116.640	3.595
2.1810	2.9480	0.000409	111.730	3.612
2.2720	2.9390	0.000393	106.640	3.633
2.3630	2.9290	0.000348	95.080	3.626
(Straight Section)				
2.4520	2.9290	0.000302	80.960	3.697
2.5410	2.9290	0.000264	69.490	3.770
2.6310	2.9290	0.000228	58.790	3.852
2.7500	2.9290	0.000205	51.870	3.915
2.8700	2.9290	0.000190	47.550	3.959
2.8980	2.9290	0.000181	44.870	3.986
3.1080	2.9290	0.000175	43.160	4.007
3.2280	2.9290	0.000170	41.750	4.023
3.3770	2.9290	0.000166	40.690	4.035
3.5260	2.9290	0.000163	39.820	4.045
3.6760	2.9290	0.000161	39.020	4.056
3.8240	2.9290	0.000157	38.270	4.066

(continued)

Table 4-1 - DIFFUSER WALL CONDITIONS (Pc = 400) Cont'd

X (ft)	R_{wall} (ft)	Density (lbm/ft^3)	Static Press. (psfa)	Mach No.
3.9730	2.9290	0.000155	37.540	4.076
4.1230	2.9290	0.000153	36.830	4.086
4.2720	2.9290	0.000150	36.130	4.097
4.4210	2.9290	0.000148	35.440	4.107
4.5700	2.9290	0.000146	34.770	4.117
4.7190	2.9290	0.000144	34.240	4.125
4.8390	2.9290	0.000142	33.720	4.133
4.9580	2.9290	0.000140	33.210	4.141
5.0770	2.9290	0.000139	32.830	4.147
5.1670	2.9290	0.000137	32.460	4.153
5.2560	2.9290	0.000136	32.100	4.159
5.3460	2.9290	0.000149	32.090	4.008
(Second Ramp)				
5.4500	2.9180	0.000163	41.130	3.946
5.5550	2.9070	0.000174	44.780	3.896
5.6590	2.8960	0.000183	47.710	3.859
5.7640	2.8850	0.000190	49.920	3.832
5.8690	2.8740	0.000194	51.450	3.813
5.9740	2.8630	0.000197	52.370	3.801
6.0800	2.8520	0.000198	52.780	3.795
6.1860	2.8410	0.000198	52.760	3.793
6.2930	2.8300	0.000197	52.400	3.794
6.4000	2.8180	0.000194	51.800	3.798
6.5070	2.8070	0.000192	51.030	3.805
6.6160	2.7960	0.000189	50.160	3.812
6.7250	2.7840	0.000186	49.260	3.821
6.8340	2.7730	0.000183	48.360	3.829
6.9450	2.7610	0.000180	47.490	3.838
7.0570	2.7490	0.000178	46.680	3.846
7.1690	2.7380	0.000175	45.930	3.853
7.2830	2.7260	0.000173	45.240	3.860
7.3980	2.7130	0.000171	44.620	3.866
7.5140	2.7010	0.000169	44.050	3.872
7.6310	2.6890	0.000167	43.530	3.877
7.7500	2.6760	0.000165	43.050	3.882
7.8710	2.6640	0.000164	42.600	3.887
7.9920	2.6510	0.000163	42.170	3.891
8.1160	2.6380	0.000161	41.770	3.895
8.2420	2.6250	0.000160	41.390	3.899
8.3690	2.6110	0.000159	41.020	3.903
8.4980	2.5980	0.000157	40.670	3.907
8.6300	2.5840	0.000156	40.330	3.911
8.7640	2.5700	0.000155	40.000	3.914
8.9000	2.5560	0.000154	39.700	3.918
9.0390	2.5410	0.000153	39.410	3.921
9.1800	2.5260	0.000152	39.130	3.924
9.3250	2.5110	0.000151	38.880	3.926

Table 4-1 - DIFFUSER WALL CONDITIONS (Pc = 400) Concl'd

S (ft)	R_{wall} (ft)	Density (lbm/ft^3)	Static Press. (psfa)	Mach No.
9.4720	2.4950	0.000150	38.640	3.929
9.6230	2.4800	0.000150	38.430	3.931
9.7770	2.4630	0.000149	38.240	3.933
9.9310	2.4470	0.000148	38.080	3.934
10.0800	2.4310	0.000148	37.960	3.935
10.2300	2.4160	0.000148	37.860	3.936
10.3700	2.4010	0.000147	37.780	3.936
10.5100	2.3860	0.000147	37.730	3.936
10.6500	2.3710	0.000147	37.700	3.936
10.7900	2.3570	0.000147	37.690	3.935
10.9200	2.3430	0.000147	37.700	3.934
11.0600	2.3290	0.000147	37.720	3.934
11.1800	2.3150	0.000147	37.770	3.932
11.3100	2.3020	0.000147	37.840	3.931
11.4400	2.2890	0.000147	37.930	3.929
11.5600	2.2760	0.000148	38.010	3.927
11.6800	2.2630	0.000148	38.130	3.925
11.8000	2.2500	0.000148	38.260	3.923
11.9200	2.2380	0.000149	38.400	3.920
12.0400	2.2260	0.000149	38.560	3.918
12.1600	2.2130	0.000150	38.740	3.915
12.2700	2.2010	0.000150	38.930	3.912
12.3800	2.1890	0.000151	39.130	3.908
12.5000	2.1780	0.000152	39.360	3.905
12.6100	2.1660	0.000152	39.600	3.901
12.7200	2.1540	0.000153	39.850	3.897
12.8300	2.1430	0.000154	40.130	3.893
12.9400	2.1310	0.000155	40.420	3.888
13.0600	2.1200	0.000156	40.740	3.884
13.2600	2.0970	0.000158	41.450	3.874
13.3700	2.0860	0.000159	41.840	3.868
13.4700	2.0750	0.000161	42.280	3.862
13.5800	2.0640	0.000162	42.760	3.855
13.7900	2.0420	0.000166	43.900	3.840
13.8900	2.0310	0.000168	44.590	3.831
14.0000	2.0200	0.000170	45.380	3.821
14.1000	2.0090	0.000173	46.320	3.808
14.2100	1.9980	0.000175	47.260	3.895
26.2100	1.9980	0.000175	47.260	3.895
38.1900	1.9980	0.001756	1087.200	0.351

(End of Second Ramp)

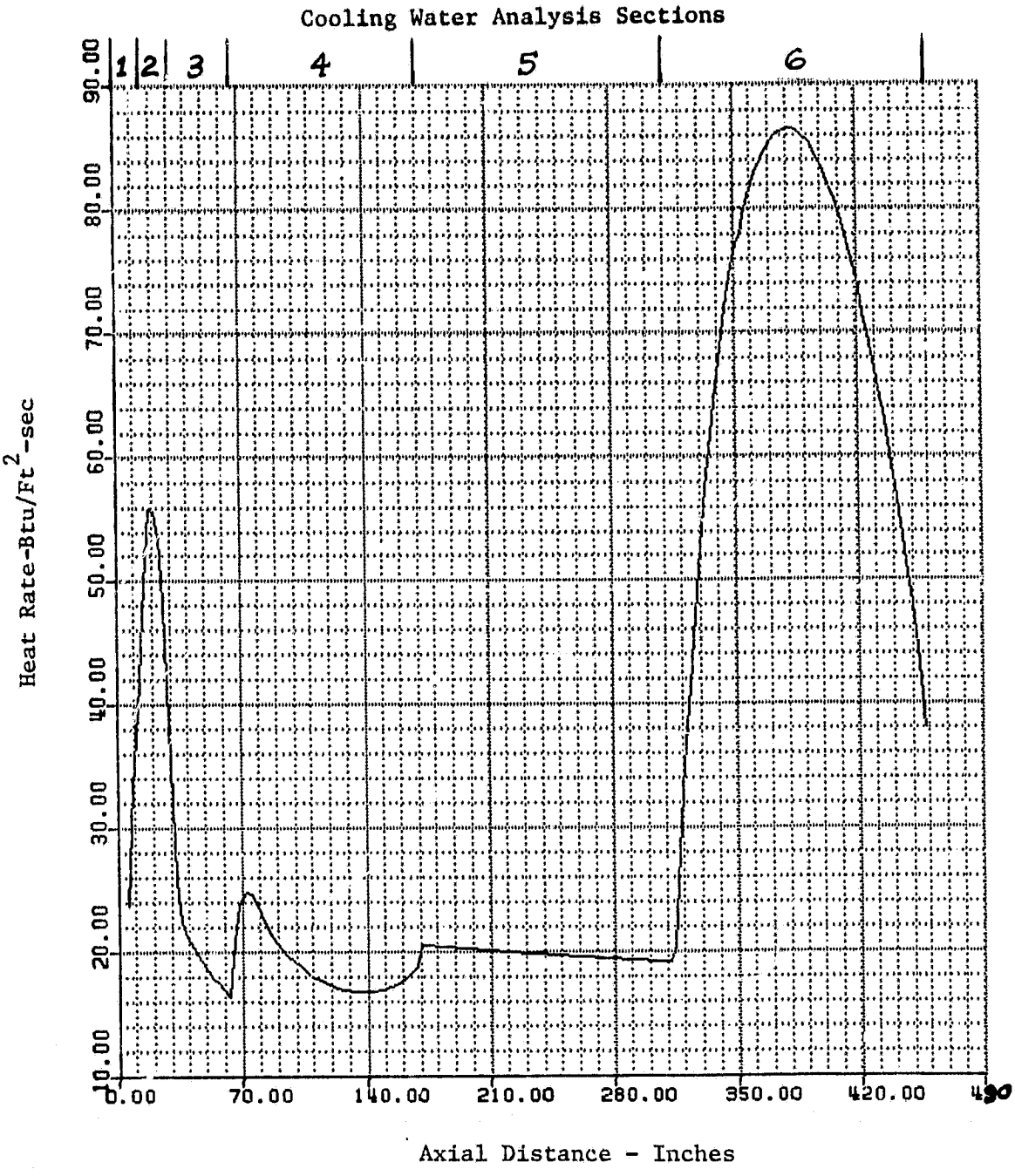

Fig. 4-7 - Diffuser Cold Wall (540 R) Heat Rate Distribution

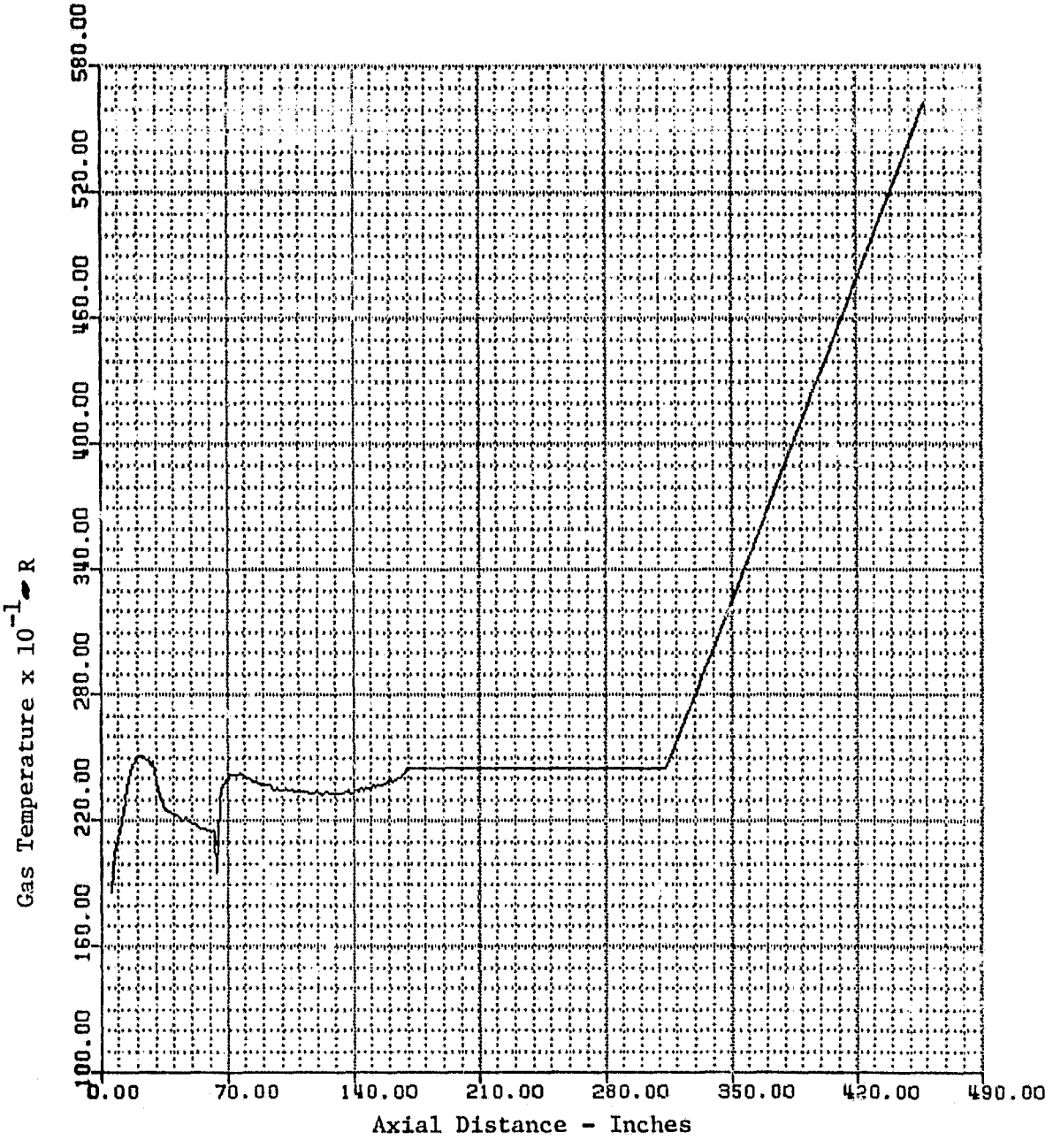

Fig. 4-8 Diffuser Local Temperature Distribution

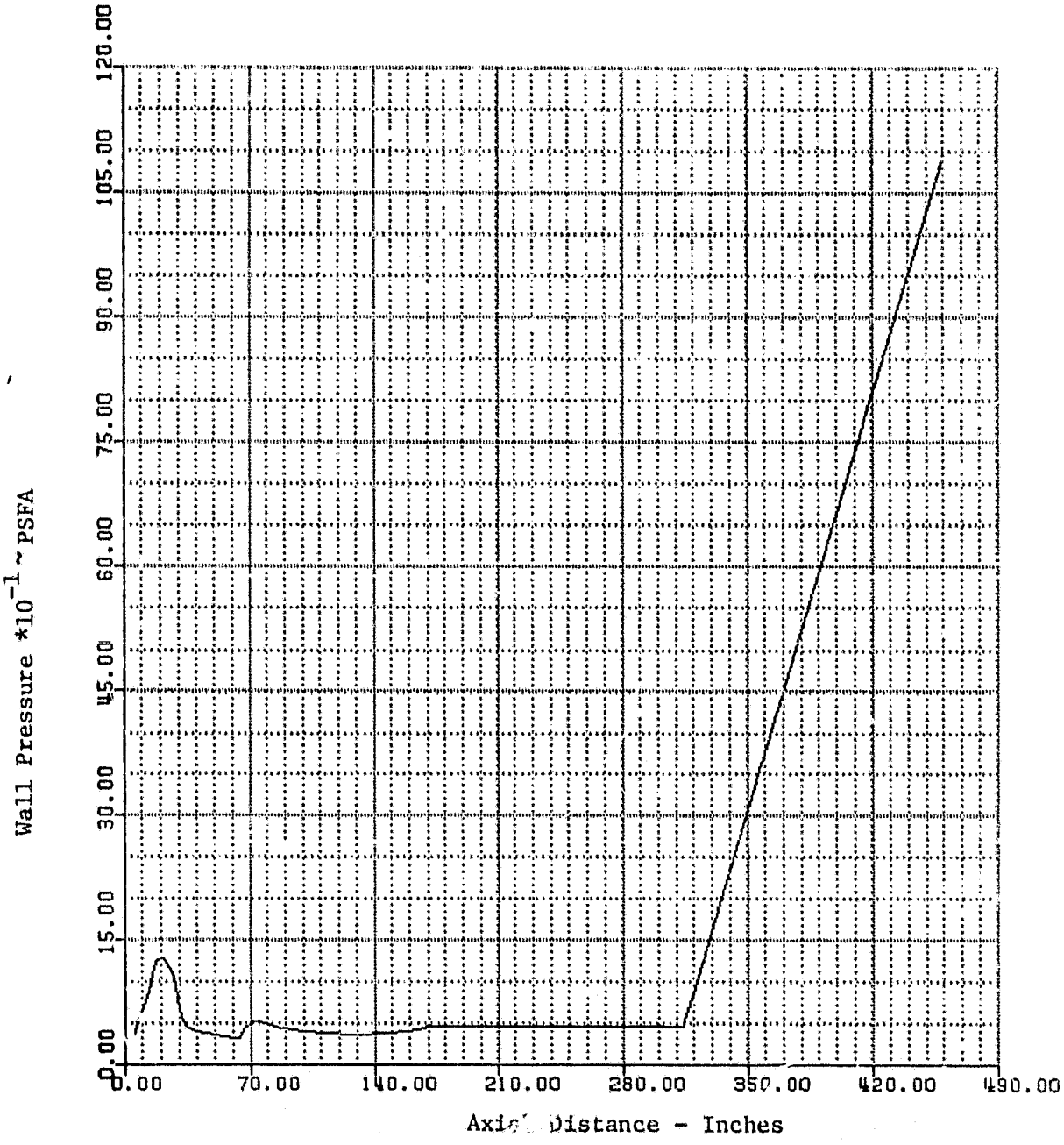

Fig. 4-9 Diffuser Local Pressure Distribution

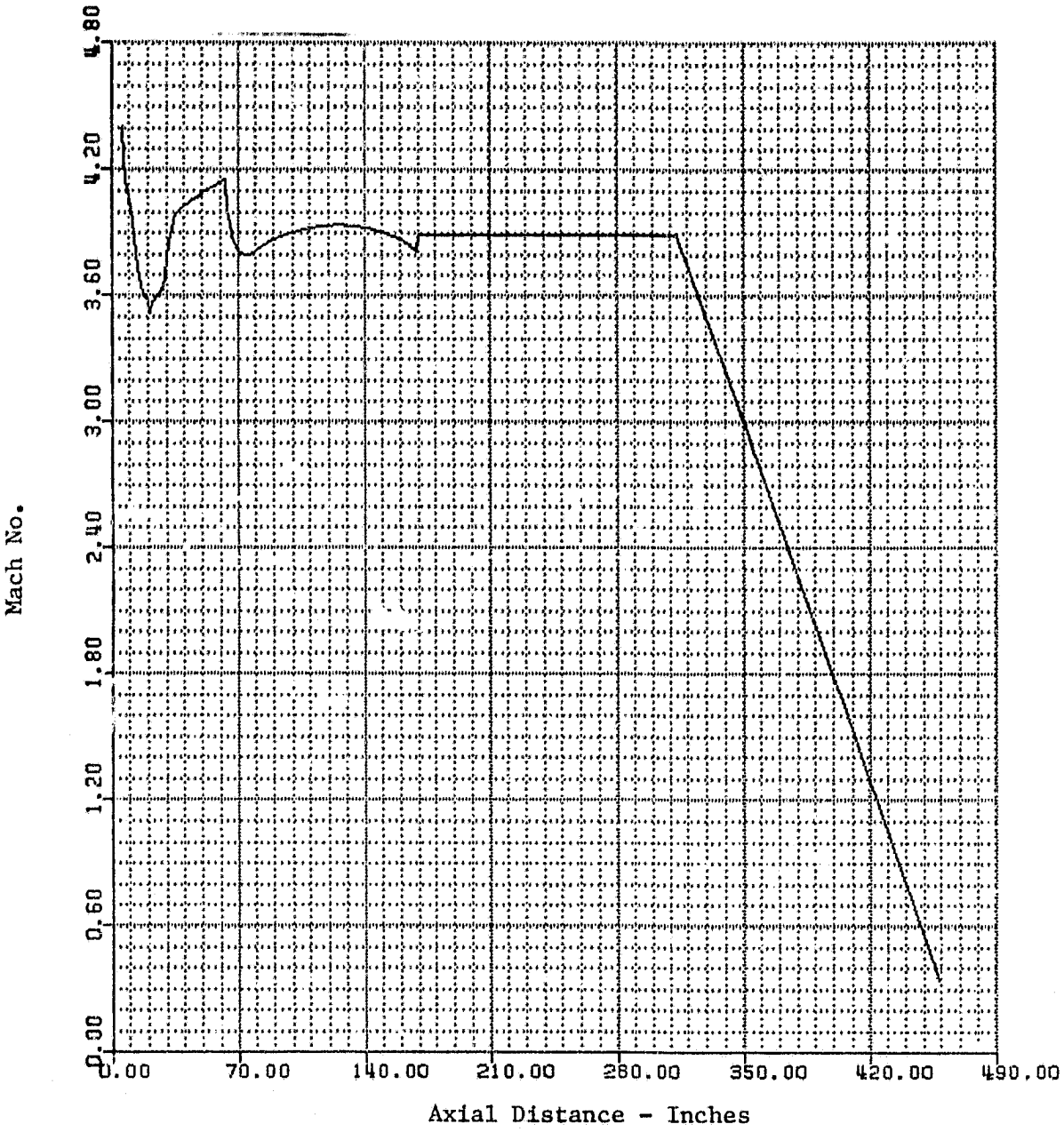

Fig. 4-10 - Diffuser Wall Mach Number Distribution

4.3.3 Diffuser Cooling Water Requirements

The diffuser was divided into six separate segments to perform the cooling water analysis. The separate segments are shown in Fig. 4-7. The results of this analysis are shown in Table 4-2. The maximum gas side film coefficient was used over the entire section. The water flow rates were designed to be the same through each section with the water bulk temperature rise being a variable as shown in the last column of Table 4-2. In this way, the same water can be used from one end to the other, starting at the ejector end. This design minimizes the water flow requirements with the total bulk temperature rise being only 71 F. The diffuser wall thickness between the hot gas side and the water was selected at 0.125 in. The wall would be structurally stiffened by the water channel ribs and the outer water channel skin. The entire diffuser could be made from mild steel sheet since the maximum gas wall temperature is only 442 F. As a result of this analysis, no thermal problems are anticipated with the diffuser.

4.3.4 Afterburning Analysis

The engine flow exiting from the diffuser tube into the first ejector contains excess H_2 gas. The ejector gas contains excess hot air. The purpose of this analysis was to determine if any appreciable afterburning would occur in the first ejector mixing tube thereby raising the temperature and possibly choking the flow. The pertinent flow variables prior to mixing are shown in Fig. 4-3. The central gas core passes a normal shock wave prior to its exit from the tube, thereby raising its temperature up to 5700 R. Also shown for comparison purposes in Fig. 4-3. are the results that were obtained using the area averaged GIM code upstream flow results and processing the flow across a normal shock. Excellent agreement (within 8% on pressure) is obtained between the 1-D DIFEJJ CODE and the GIM code for the main engine flow exiting the diffuser tube.

The laser And Mixing Program (LAMP) Ref. 29, was used to perform the afterburning analysis. This program has been used in the past by Lockheed to study the Space Shuttle main engine (SSME) exhaust/ambient air mixing phenomena and good comparisons were obtained with the available measured data. Since

Table 4-2 – SUMMARY RESULTS OF DIFFUSER COOLING WATER REQUIREMENTS

Section Number	$\dot{Q}_{MAX}$ Btu/Ft^2-Sec	Maximum Gas Side Film Coeff. Btu/Ft^2-Sec-R	Water Side Film Coeff. Btu/Ft^2-Sec-R	Water Velocity Ft/Sec	Heat Area Ft^2	Gas Side Wall Temp. °F	Water Side Wall Temp. °F	Water Flowrate GPM	Water Press. Drop PSF	Water Bulk ΔT °F
1 and 2	56	.012	.4252	5	36	343	275	2345	11	6
3	30	.0064	.4252	5	55	255	218	2345	17	5
4	25	.0053	.4252	5	138	240	206	2345	51	11
5	20	.0043	.4252	5	150	221	196	2345	70	9
6	87	.0185	.4252	5	150	442	338	2345	70	40

Notes

1) Diffuser wall material is 0.125 in. thick mild steel

2) $\dot{Q}$ MAX based on 80°F wall temperature

the SSME uses the identical propellant system as the RL10-IIB, the same finite rate chemistry package was used in this analysis.

The results obtained are subject to the following assumptions:

1. Mixing and reactions proceed at constant pressure.
2. Due to the current setup of the LAMP code for axisymmetric mixing, conditions on the outermost streamline (i.e., the outer edge of the ejector flow) will remain constant. This implies a constant ejector wall temperature, as well as constant velocity and gas composition along the wall.

The results indicated that no appreciable afterburning will occur and that the effect of the ejector flow is to cool the hot diffuser gas with a subsequent flow area reduction.

4.3.5 Engine/Diffuser Startup Transients

During the RL10-IIB engine startup transient which takes about 3 sec, the H_2 fuel leads the oxidizer. The fuel flow builds up to a maximum of 5.0 lbm/sec in 3 sec duration. During this time the igniter is firing. Combustion will not occur until a minimum of 4 psia chamber pressure is reached in the presence of some oxidizer. The concern is what happens when the leading H_2 fuel reaches the relatively warm turbojet oxygen-rich exhaust. This problem is shown pictorially in Fig. 4-11. As can be seen in the figure, the ejector blank-off conditions in the diffuser tube are pressure = 0.068 psia and temperature of 429R. This condition will not promote detonation of the H_2 fuel. The H_2 fuel will be mixed with the ejector flow and swept downstream and burned. To absolutely preclude any possibility of detonation, a purge flow of N_2 has been added as shown in Fig. 4-11 and previously in Fig. 3-3.

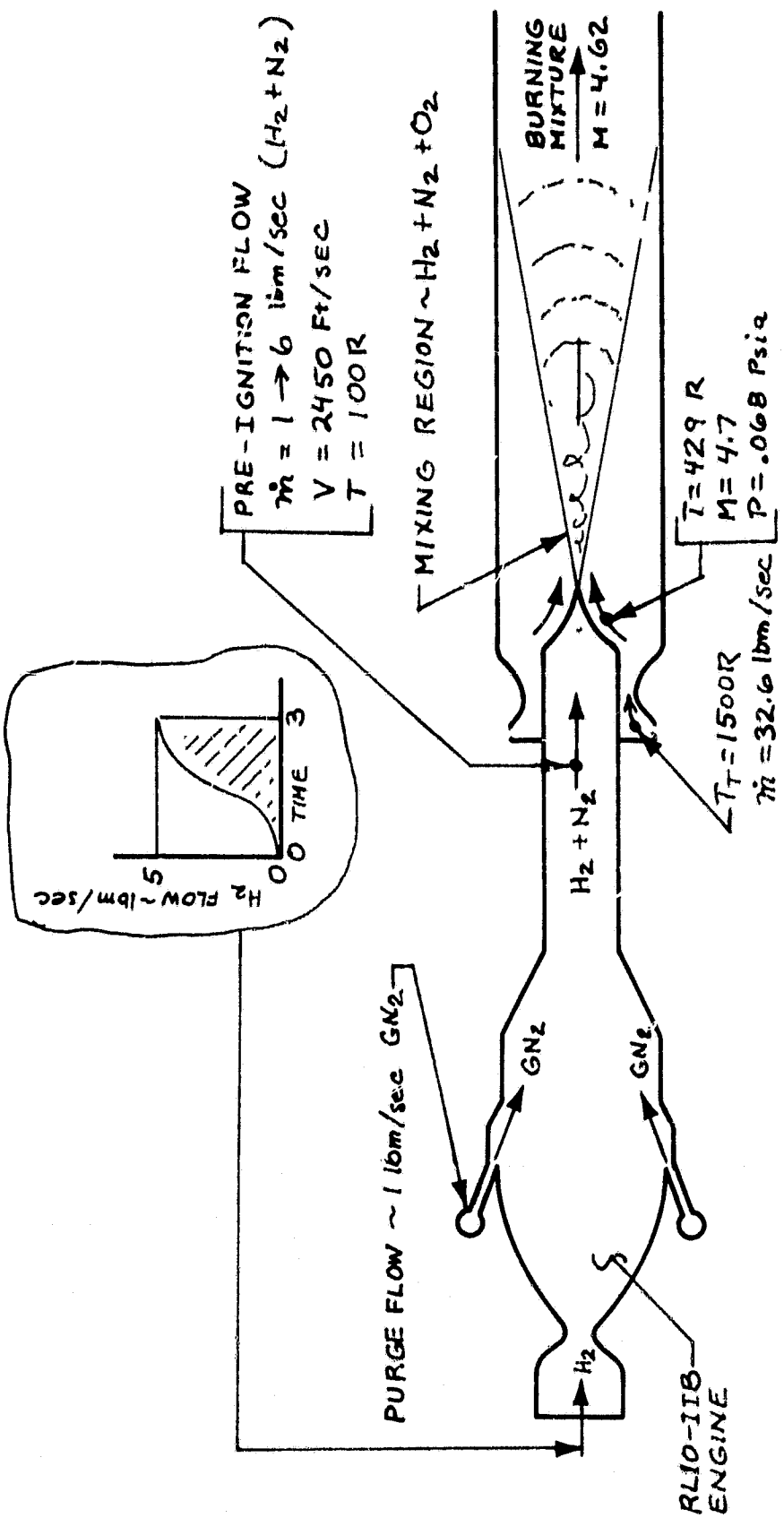

Fig. 4-11 - Pictorial Presentation of RL10-IIB Engine Startup Transients

5. CONCLUSIONS

As a result of this contract, a very useful diffuser/ejector design computer program was developed. Using empirically modified one-dimensional flow methods the diffuser ejector geometry is specified by the code. Results obtained using the detailed GIM code verified the design code results for calculations up to the end of the diffuser second throat.

This study has demonstrated that through careful extrapolation of existing analytical methods and experimental data, a two-stage diffuser/ejector building block system can be designed which will accommodate any potential OTV space engine.

The results of this study have demonstrated that through careful design, an ejector system using two commonly available turbojet engines feeding two variable area ratio ejectors is indeed feasible. In fact, the use of turbojet engines as ejector drivers is much more practical than the use of steam.

This study has defined diffuser requirements for sea level testing of high expansion ratio space engines. The analysis has demonstrated numerically the practicality and feasibility of a "building block" engine diffuser/ejector system. The next step would be to define and evolve the design further and study the possibility of building a prototype system. However, due to scale model boundary layer effects, a prototype system smaller than 1/4 scale may not provide meaningful results.

Future analytical effort should involve additional GIM code analysis of the two stage ejector mixing process.

REFERENCES

1. Wojciechowski, C. J., "Preliminary Study of the Diffuser Design Requirements for Sea Level Testing of the ASE and Expansion Cycle Engines," LMSC-HREC TN D697618, Lockheed Missiles & Space Company, Huntsville, Ala., 17 July 1979.

2. Wojciechowski, C. J., "Preliminary Study of the Diffuser Design Requirements for Sea Level Testing of the ASE 200:1 and 175:1 Engines," LMSC-HREC TN D697765, Lockheed Missiles & Space Company, Huntsville, Ala., December 1979.

3. Taylor, D., and F. R. Toline, "Summary of Exhaust Gas Ejector-Diffuser Research," AEDC-TR-68-84, October 1968.

4. Roschke, E. J., P. F. Massier and H. L. Grier, "Experimental Investigation of Exhaust Diffusers for Rocket Engines," TR 32-310, Jet Propulsion Laboratory, Pasadena, Calif. 15 March 1962.

5. "Liquid Rockets and Propellants," Progress in Astronautics and Rockertry, Vol. 2, pp. 3-118, Library of Congress Card Catalog No. 629.4 P94 V.2.

6. Massier, P. F. and E. J. Roschke, "Experimental Investigation of Exhaust Diffusers for Rocket Engines," TR 34-59, Jet Propulsion Laboratory, Pasadena, Calif., 5 May 1960.

7. Hale, J. W., and W. C. Gobbell, "Diffuser Auxiliary Ejector Development for the Design of the J-3 LEM Descent Exhaust System," AEDC-TR-65-255, February 1966.

8. Shapiro, Ascher H., The Dynamics and Thermodynamics of Compressible Fluid Flow, Vol. I, pp. 135, 151 and pp. 173-178, Vol II, pp. 691-692, pp. 1153-1156.

9. German, R. C., and R. C. Bauer, "Effects of Diffuser Length on the Performance of Ejectors without Induced Flow," AEDC-TN-61-89 (AD 262 888), August 1961.

10. Bauer, R. C., and R. C. German, "Some Reynolds Number Effects on the Performance of Ejectors without Induced Flow," AEDC-TN-61-87 (AD 262 734), August 1961.

11. Fabri, J., and J. Paulon, "Theory and Experiments on Supersonic Air-to-Air Ejectors," NACA-TM-1410, September 1958.

12. Bauer, R. C., and R. C. German, "The Effect of Second-Throat Geometry on the Performance of Injectors without Induced Flow," AEDC-TN-61-133 (AD 267 263), November 1961.

13. Jones, William L., H. G. Price, Jr., and C. F. Lorenzo, "Experimental Study of Zero-Flow Ejectors Using Gaseous Nitrogen," NASA-TN D-203, March 1960.

14. Panesci, J. J., and R. C. German, "An Analysis of Second Throat Diffuser Performance for Zero-Secondary-Flow Ejector Systems," AEDC-TDR-63-249 (AD 426 336), December 1963.

15. Lynch, G. R., and C. T. Carman, "An Investigation of the Performance of a Hot-Gas Jet Pump With and Without Induced Flow," AEDC-TDR-64-234 (AD 452 985), December 1964.

16. Hale, J. W. and W. C. Bobbell, "Diffuser Development for Throttlable Engines," AEDC-TR-65-7 (AD 458 437), March 1965.

17. Bauer, R. C., "Theoretical Base Pressure Analysis of Axisymmetric Ejectors without Induced Flow," AEDC-TDR-64-3 (AD 428 633), Jan. 1964.

18. Taylor, D., and D. L. Barton and M. Simons, "An Investigation of Cylindrical Ejectors Equipped with Truncated Conical Inlets - Phase II," AEDC-TN-60-224 (AD 252 643), March 1961.

19. Korst, H. W., and W. L. Chow, "Compressible Non-Isenergetic Two-Dimensional Turbulent (P_{r_t} = 1) Jet Mixing at Constnat Pressures," University of Illinois Engineering Experiment Station, ME-TN-392-4, (AD 211 328), January 1959.

20. Taylor, D., R. C. Bauer, and M. Simmons, "A Technique for Producing Very Low Ambient Densities in Ground Test Facilities during Tests of Rocket Engines," AEDC-TR-65-14 (AD 457 893), February 1965.

21. Peters, C. E., and S. Wehofer, "Theoretical Performance of Air-Driven Ejectors for Pumping Rocket Exhaust Gases," AEDC-TDR-62-134 IAD 277 056), June 1962.

22. German, R. C., R. C. Bauer, and J. H. Panesci, "Methods for Determining the Performance of Ejector-Diffuser Systems," Journal of Spacecraft and Rockets, Vol. 3, No. 2, February 1966, pp. 193-200.

23. Hale, J. W., "Influence of Pertinent Parameters on Ejector-Diffuser Performance With and Without Ejected Mass," AEDC-TDR-64-134 (AD 602 770), July 1964.

24. Hasinger, S. H., and A. C. Draper, "Comparison of Experiment and Analysis for a High Primary Mach Number Ejector," AFFDL-TR-77-38, May 1977.

25. S. H. Hasinger, "Ejector Optimization," AFFDL-TR-78-23, June 1978.

26. Svehla Roger A., "Thermodynamic and Transport Properties for the Hydrogen-Oxygen System," NASA SP-3011 (1964).

27. Spardley, L. W., and P. G. Anderson, "The General Interpolants Method," AIAA Paper 77-642, Third Computational Fluid Dynamics Conference, Albequerque, NM, June 1977.

28. Blackledge, M. L., and C. J. Wojciechowski, "Real Gas Multiple Pressure Gradient Heating Rate Program," LMSC-HREC A783781, Lockheed Missiles & Space Company, Huntsville, Ala., May 1967.

29. Thoenes, J., et. al., "Laser and Mixing Program (LAMP) Theory and User's Guide," Lockheed Missiles & Space Company, Huntsville, Alabama, Technical Report RH-CR-77-4, August 1966.

Appendix A

DIFFUSER BOUNDARY LAYER HEAT TRANSFER THEORY

NOMENCLATURE FOR APPENDIX A

Symbols

C_p	specific heat at constant pressure, Btu/lb-^oR
g_h	enthalpy conductance, lbm/ft^2-sec
h_r	adiabatic wall enthalpy, Btu/lb
J	conversion factor, 778 ft-lb/Btu
Nu	Nusselt number, dimensionless
Pr	Prandtl number, dimensionless
q	convective heat transfer rate, Btu/sec-ft^2
r	recovery factor, dimensionless
Re	Reynolds number, dimensionless
S	distance along a flow streamline, ft
T	temperature, ^oR
V	velocity, ft/sec
X_L	flow characteristic length, ft

Greek

ϵ	shape factor, ft
η	cone half angle, deg
ρ	density, lb/ft^3

Subscripts

e	property evaluated at the edge of the boundary layer
r	property evaluated at the defined reference condition
w	property evaluated at the wall

Appendix A

In this Appendix, the boundary layer heat transfer theories used in the diffuser heat load analysis are presented.

- Laminar Boundary Layer

Heat transfer through a laminar boundary layer is calculated using the integral form of the energy equation. Effects of variable freestream velocity, density, and pressure are accounted for through use of appropriate transforms of the flat plate solution. Non-constant properties through the boundary layer are also accounted for.

In Ref. A-1 (among others) it is shown that the energy equation can be reduced to an equation with enthalpy as the dependent variable under a number of different conditions including some cases where there is dissociation, chemical reaction and mass diffusion within the boundary layer. The complete development of the enthalpy form of the equation and the evaluation of the surface heat rate are presented in Ref. A-1.

Based on examination of several "exact" laminar boundary layer solutions, Eckert (Ref. A-2) recommends that the effects of variable gas properties through the boundary layer can be accounted for by simply evaluating the properties at a "reference enthalpy" and using these values in the constant property solutions as obtained by Blasius. Based on this method, the convective heat rate to the wall is evaluated using

$$\dot{q} = g_h(h_r - h_w), \qquad \text{A-1}$$

where the adiabatic wall or recovery enthalpy is

$$h_r = \int_o^{T_e} c_p \, dT + \frac{r V_e^2}{2 J g} \quad , \tag{A-2}$$

where

$$r = \sqrt{Pr^*} \quad . \tag{A-3}$$

The enthalpy conductance g_h is evaluated from the Stanton number (St)

$$St^* = \frac{g_h}{\rho^* V_e} = \frac{Nu^*}{Re^* Pr^*} \quad . \tag{A-4}$$

The starred (*) properties refer to properties evaluated at a temperature corresponding to a "reference enthalpy," h*, where

$$h^* = h_e + 0.5 (h_w - h_e) + 0.22 (h_r - h_e) \, . \tag{A-5}$$

It can be readily seen that an iterative solution is required for Eqs. (A-2), (A-3) and (A-4).

The Blasius flat plate constant-property boundary layer solution yields

$$\frac{Nu}{\sqrt{Re}} = 0.332 \, Pr^{1/3} \quad . \tag{A-6}$$

Substituting Eq. (A-6) into (A-4) yields

$$g_h = \frac{0.332}{Pr^{*2/3}} \frac{\rho^* V_e}{\sqrt{Re^*}} \quad . \tag{A-7}$$

Substituting, $Re^* = \frac{\rho^* V_e X_L}{\mu^*}$, and Eq. (3.80) into Eq. (A-1) yields

$$\dot{q} = \frac{0.332}{Pr^{*2/3}} \frac{(\rho^* \mu^* V_e)^{0.5}}{X_L^{0.5}} (h_r - h_w) \cdot \qquad \text{(A-8)}$$

The characteristic length (X_L) as used in Eq. (A-8) is obtained for variable property flow by numerically integrating the following equation along a flow-field streamline, (Refs. A-1 through A-3).

$$X_L = \frac{1}{\rho^* \mu^* V_e \epsilon^2} \int_o^S \rho^* \mu^* V_e \epsilon^2 \, dS. \qquad \text{(A-9)}$$

The parameter S is the wetted length along the streamline. For a flat plate the parameter ϵ is set equal to a constant and thereby divided out, and for constant inviscid flow properties, the characteristic length (X_L) becomes equal to the flat plate length. For axisymmetric flow about a cone with constant inviscid properties, the equivalent length, X_L, becomes

$$X_L = \frac{1}{\epsilon^2} \int_o^S \epsilon^2 \, dS.$$

For a cone with a cone half angle of η, the parameter ϵ is the local cone radius, i.e.,

$$\epsilon = r = S \tan\eta \,,$$

and the equivalent length becomes

$$X_L = \frac{1}{S^2 \tan^2\eta} \int_o^S S^2 \tan^2\eta \, dS = \frac{S}{3}. \qquad \text{(A-10)}$$

The method used to calculate the gas transport properties is based on the Lennard-Jones potential intermolecular force model as discussed in Ref. A-4.

- Turbulent Convective Heat Transfer

A similar method of analysis is used in this case as in the laminar case previously discussed and is presented in Ref. A-1 and A-5. The basic heat transfer equation to be solved is Eq. (A-1). The Stanton number defined by Eq. (A-4), for turbulent flow becomes (Refs. A-1, A-2 and A-5).

$$St = 0.0296\, Re_x^{-0.2}\, Pr^{-2/3}. \qquad (A\text{-}11)$$

Substitution of Eq. (A-11) into Eq. (A-4), yields the enthalpy conduction g_h as

$$g_h = \frac{0.0296}{Pr^{2/3}} (\rho V_e)^{0.8} \left(\frac{\mu}{X}\right)^{0.2}. \qquad (A\text{-}12)$$

Substitution of Eq. (A-12) into Eq. (A-1) and using the characteristic length (Ref. A-5) to account for nonuniform inviscid flow the turbulent flow convective heat transfer equation becomes,

$$q = \frac{0.0296}{Pr^{*.66}} (\rho^* V_e)^{0.8} \left(\frac{\mu^*}{X_T}\right)^{0.2} (h_r - h_w). \qquad (A\text{-}13)$$

The starred parameters density, viscosity and Prandtl number are again calculated at a reference temperature corresponding to the Eckert reference enthalpy Eq. (A-5). The Eckert reference enthalpy is calculated as in the laminar case except that the recovery factor, r, is

$$r = Pr^{*\,1/3}.$$

The recovery enthalpy is calculated using Eq. (A-2).

The stretched characteristic length, X_T is defined (Ref. A-5) by

$$X_T = \frac{1}{\rho^* \mu^* V_e \epsilon^{1.25}} \int_o^S \rho^* \mu^* V_e \epsilon^{1.25} \, dS, \qquad (A-14)$$

where S is the distance along the streamline.

For a flat plate, the parameter ϵ is set equal to a constant and thereby divided out, and for constant inviscid flow properties, the characteristic length X_T becomes equal to the flat plate length.

For a cone with a cone half angle of η, the parameter ϵ is equal to the cone local radius and is defined by

$$\epsilon = r = S \tan\eta \, .$$

For constant inviscid flow properties, the characteristic length X_T becomes

$$X_T = \frac{1}{S^{1.25} \tan^{1.25}\eta} \int_o^S S^{1.25} \tan^{1.25}\eta \, dS = \left(\frac{4}{9}\right) S \, .$$

REFERENCES

A-1 Kays, W.M., Convective Heat and Mass Transfer, Chap. 14, McGraw-Hill, New York, 1966.

A-2 Eckert, E.R.G., "Engineering Relations for Friction and Heat Transfer to Surfaces in High Velocity Flow," J. Aerospace Sci., August 1955, pp. 585-587.

A-3 Vaglio-Laurin, R., "Laminar Heat Transfer on Blunt-Nosed Bodies in Three-Dimensional Hypersonic Flow," WADC TN 58-147, Wright-Patterson AFB, Ohio, May 1958.

A-4 Hirschfelder, J. O., C. F. Curtiss and R. B. Bird, Molecular Theory of Gases and Liquids, Wiley, New York, 1964.

A-5 Vaglio-Laurin, R., "Turbulent Heat Transfer on Blunt-Nosed Bodies in Two-Dimensional and General Three-Dimensional Hypersonic Flow," J. Aerospace Sci., January 1960.